SLAC-PUB-1231
(I)
April 1973

A POLARIZED PHOTON BEAM PRODUCED BY COHERENT PAIR PRODUCTION IN ORIENTED GRAPHITE*

R. L. Eisele, D. J. Sherden, R. H. Siemann+, C. K. Sinclair
Stanford Linear Accelerator Center
Stanford University, Stanford, California 94305

D. J. Quinn, J. P. Rutherfoord, M. A. Shupe
Tufts University, Medford, Massachusetts 02155

Abstract

Attenuation by coherent pair production in highly oriented, compression annealed, pyrolytic graphite has been used to polarize a 16-GeV bremsstrahlung beam. The polarizer consists of 61 cm of graphite crystals whose reciprocal lattice vectors are oriented at 10.5 mrad to the normal to the beam direction, and can be rotated by 90^{o} about the beam line to rotate the plane of polarization. A functionally identical assembly of length 30.5 cm was used as an analyzer to measure the polarization of the beam with the SLAC pair spectrometer. The beam produced intensities greater than 4×10^{8} equivalent quanta per beam pulse and had a measured polarization of 0.255 ± 0.020.

(Submitted to Nucl. Instr. and Methods.)

---

*Work supported by the U. S. Atomic Energy Commission.

+Present address: Brookhaven National Laboratory, Upton, New York 11973

1. Introduction

Polarized photons have proved extremely useful in the detailed study of photoproduction mechanisms. At different energies and for different processes, questions about nucleon isobar production, helicity conservation, or the parity sequence (whether natural or unnatural) of exchanges can be answered.

Because of their usefulness, numerous techniques have been developed to produce polarized photons. To study reactions with relatively small cross sections[1] one needs an intense beam and experimental techniques which selectively look at the process of interest. Prior to the beam discussed here, only a coherent bremsstrahlung beam[2-4] had the necessary intensity.

However, there are difficulties associated with the use of a coherent bremsstrahlung beam, and these prompted construction of the beam discussed here. Both the intensity and the polarization of the polarized enhancement go to zero as the energy of the enhancement approaches the energy of the incident electron beam. The energy (k) of the photons of interest must then be chosen well below the end-point energy (E_0) of the beam, typically at k/E_0 between 0.5 and 0.75. There is always a spectrum of unpolarized photons, similar to a bremsstrahlung spectrum from an amorphous radiator, above the polarized photon spike. The spectrum of a coherent bremsstrahlung beam with $k/E_0 = 0.5$ is shown in Fig. 1.

Because these higher energy photons contribute to the measured yield, one must know the energy of the photon producing an event of interest. This can be done by detecting the final state particles in coincidence[3] or by utilizing the sharp energy dependence of the beam spectrum in the enhanced region.[4] Each of these techniques has difficulties, the former because of complex final states and/or poor accelerator duty cycle, and the latter because of tight (but achievable) tolerances on both mechanical components and beam phase space and because of a large background from the higher energy photons. Independent of the solution,

the problem is the presence of the unpolarized higher energy photons.

In 1962, Cabibbo et al.[5] suggested polarizing photons by coherent pair production in crystals, and in 1970 Berger et al.[6] successfully tested this method. The essence of this technique is that an initially unpolarized photon beam is passed through a crystal and attenuated by coherent pair production. The lattice vectors of the crystal are oriented such that photons of one polarization are attenuated more than those of the other. The beam which emerges from the crystal is then a reduced intensity polarized beam with a modified bremsstrahlung function. Because the process works through attenuation rather than production of photons, the polarization as a function of energy depends only on the crystal orientation and not on the spectrum or end-point energy of the incident beam. It therefore becomes possible to polarize photons at the maximum energy of the spectrum. In addition to removing the principal background associated with the coherent bremsstrahlung beam, one can perform experiments at the highest achievable energy. Furthermore, the maximum polarization obtainable for a fixed length of crystal can be shown to increase as the beam energy is increased.

Following the successful test of Berger et al.[6] we began construction of such a polarized photon beam at SLAC. This beam has been successfully used in an experiment to study pseudoscalar meson photoproduction.[7] This paper describes the design, construction, and properties of the beam.

2. Coherent pair production

Coherent pair production and bremsstrahlung have been discussed in the literature[2,5] and it is not our purpose to review the subject in detail. Rather we wish to present only useful concepts and details relevant to the design and performance of the beam.

A. General remarks

For a photon of energy k to produce an electron-positron pair (let m = electron mass) with energies E^+ and E^- (define $y = E^+/k$), there must be momentum transfer q to a nucleus or crystal lattice. This momentum transfer has components $q_{\parallel}$ parallel and $\underline{q}_{\perp}$ perpendicular to the photon direction. For pair production to be kinematically possible, it is necessary that $q_{\parallel}$ be greater than a minimum

$$q_{\parallel} > \delta = \frac{m^2}{2ky(1-y)} \quad . \tag{1}$$

The cross section decreases rapidly as $q_{\parallel}$ increases from this minimum and, therefore, most pair production occurs with $q_{\parallel} \simeq \delta$. If $\underline{g}$ is a reciprocal lattice vector of a crystal, coherent pair production occurs when

$$|\underline{g}| \theta \simeq \delta \tag{2}$$

where θ is the angle of $\underline{g}$ with respect to the normal to the photon direction.

The cross section for pair production by a photon with polarization vector perpendicular to $\underline{q}_{\perp}$ is greater than that for a photon polarized parallel to $\underline{q}_{\perp}$. The asymmetry for pair production goes to zero when either the electron or positron has most of the photon energy, and the net asymmetry is dominated by pair production with $y \sim 1/2$ (see Fig. 2), where the electron and positron equally share the photon energy. Using $y \sim 1/2$ and $q_{\parallel} \simeq \delta$, one obtains from Eq. 1 and 2 that the polarization is greatest for photons of energy

$$k \sim \frac{2m^2}{|\underline{g}|\theta} \quad . \tag{3}$$

B. Oriented graphite

The beam described in this paper used compression annealed pyrolytic graphite crystals.[8] The density of the crystal is 2.26 g/cm^3 and the crystalline

interlayer spacing is 3.355 - 3.357 Å.[9] Because there is no ordering in the a-axis dimensions of these crystals, they behave as crystals only in the c-axis dimension, making all the reciprocal lattice vectors parallel. Hence the crystal orientation, and consequently the polarization at a given energy, can be described by a single angle θ.

To determine the properties of the beam, one must calculate the coherent and incoherent pair production cross sections for a fixed energy partition y and orientation θ; the coherent cross section is the sum of the cross sections from all reciprocal lattice vectors. These cross sections depend on the effective Debye temperature, which is taken to be 530° K,[10] and the carbon form factor (we use the free carbon form factor).[11] Typical cross sections are shown in Fig. 2. These cross sections are then integrated over the energy partition to give the cross sections as a function of θ only (see Fig. 3).

Due to crystal and crystal holder imperfections and to beam divergence (crystal imperfections are dominant in our case), the angle θ is not fixed but has a distribution of finite width. The mosaic spreads, as measured by x-ray diffraction, have average values between 5.58 mrad and 6.63 mrad (FWHM).[12] To account for other crystal imperfections (gross warpage, etc.), it is necessary to add approximately 1.7 mrad to the mosaic spread.[13] We have assumed that the distribution in θ is Gaussian with FWHM = 8.03 mrad. This distribution is then folded into the cross sections to give the calculated beam properties. Figure 4 shows the resultant cross sections. All of the calculations of the beam properties presented here were obtained from a computer program written by D. Gustavson and R. Schwitters.[14]

The results one calculates in this manner are sensitive to the parameters used. Berger et al.[6] could not obtain agreement between experiment and

calculation without modifying the carbon form factor (we have not retained their modification). Their results clearly show the necessity of measuring the important properties of the beam. Calculations as described above are useful in showing qualitative behavior as parameters are varied, but cannot be relied upon for precise quantitative results.

3. Design considerations

Many of the basic design features of the polarizer come from the basic features of coherent pair production. More detailed considerations, such as angular tolerances, come from the calculations described above.

A. Basic design features

In performing a polarized photon experiment, the measured asymmetry (defined for pseudoscalar meson photoproduction) is given by

$$\Sigma_m = \frac{\sigma_\perp - \sigma_\parallel}{\sigma_\perp + \sigma_\parallel} = P\Sigma \qquad (4)$$

where Σ is the physical asymmetry of the photoproduction reaction, P is the beam polarization, and $\sigma_\perp$ ($\sigma_\parallel$) is the cross section for the photoproduction process with the beam polarization vector perpendicular (parallel) to the production plane defined by the incoming beam direction and the outgoing detected particle. To measure an asymmetry, it is, therefore, necessary to change the polarization vector with respect to the fixed production plane. Since all of the reciprocal lattice vectors of the graphite are parallel, one must then rotate the crystals by 90° about the beam direction (see Fig. 5).

The high cost of the crystals (proportional to the total volume) made it desirable to minimize the total cross-sectional area. A total crystal length of 61 cm (see below) was used, and the crystals needed to be tilted approximately 10

mrad relative to the beam axis. This tilt for a single crystal would significantly increase the required cross-sectional area over that necessary for many short assemblies, each separately oriented with respect to the beam. Therefore, the total length was achieved by using many 5.08 cm long subassemblies rather than a single crystal. The cross-sectional area was also minimized by placing the crystals as close as possible to the bremsstrahlung radiator.

The entire assembly was placed in a magnetic field to sweep the produced pairs out of the beam. This was necessary to prevent the beam spectrum from being dominated by subsequent bremsstrahlung from the pairs and to minimize the heat deposited in the crystals. Even with the sweeping magnet on, 300 - 400 watts were absorbed by the crystals. The coherent and incoherent pair production cross sections are weakly temperature dependent. The temperature derivative of the polarization is calculated to be

$$\frac{1}{P}\frac{dP}{dT} = 6.4 \times 10^{-4}/^{o}K \quad . \tag{5}$$

Hence a 15^{o} K temperature change causes the polarization to change by 1% of itself. While this is not a strong temperature dependence, the crystals needed to be cooled to prevent large temperature rises. This was accomplished by mounting each crystal in a water-cooled aluminum cart.

The beam polarization had to be measured because of the inadequacy of the calculations. In principle this could be done by measuring any process with a known asymmetry. However, the only process with a well known asymmetry at these energies, the decay asymmetry of ρ_0 photoproduction, requires coincidence detection and is difficult to measure at SLAC. The polarization could also be measured by using a second crystal to analyze the polarization of the first, and this technique was chosen. This then required that a second assembly be constructed with identical independent motions.

B. Specific design considerations

If an initially unpolarized beam is incident on the crystals, the intensities of the two polarizations at a given energy after the crystals are given by

$$I_{\perp} = \frac{I_0}{2} e^{-x_{\perp}\ell} \quad \text{and} \quad I_{\parallel} = \frac{I_0}{2} e^{-x_{\parallel}\ell} \quad . \tag{6}$$

The subscripts $\perp$ and $\parallel$ refer to the polarization vector with respect to $\underline{q}_{\perp}$ (note we use perpendicular and parallel differently here than in Eq. (4)). I_0 is the incident intensity, $x_{\perp}$ and $x_{\parallel}$ are the pair production cross sections (in units of inverse length), and ℓ is the crystal length. The polarization of the beam is given by

$$P = \frac{I_{\parallel} - I_{\perp}}{I_{\parallel} + I_{\perp}} = \frac{e^{-x_{\parallel}\ell} - e^{-x_{\perp}\ell}}{e^{-x_{\parallel}\ell} + e^{-x_{\perp}\ell}} = \tanh\left(\frac{\Delta}{2}\right) , \tag{7}$$

where

$$\Delta = x_{\perp}\ell - x_{\parallel}\ell \, . \tag{8}$$

The beam intensity after the crystal is

$$I = I_{\parallel} + I_{\perp} = \frac{I_0}{2}\left(e^{-x_{\parallel}\ell} + e^{-x_{\perp}\ell}\right) \quad . \tag{9}$$

The difference between the two cross sections and the length of the crystals determine the beam polarization. The combination of the two cross sections and the length of the crystals determine the intensity of the beam. One can obtain any desired polarization at the cost of reduced intensity.

Under the assumption that there is no upper limit on the usable beam intensity, the statistical error on the measured asymmetry per unit of beam can be optimized by maximizing IP^2 as a function of length. At 16 GeV this optimum

is at 40 cm, corresponding to a beam polarization of 15%. However, systematic errors have not been included in this optimization, and these tend to favor a higher polarization. Furthermore, if experiments are limited by the maximum tolerable rather than attainable beam intensity, the higher polarization is also desirable. Consequently a length of 61 cm (3.18 radiation lengths) was chosen for the polarizing crystals. The length of the available sweeping magnet (and the cost of the crystals) then limited the length of the analyzing crystals to 30.5 cm.

Many of the tolerances for the crystal assembly came from consideration of possible errors. In particular, care was taken to avoid differences in either the shape of the beam spectrum or the beam polarization when the crystals were rotated through 90°. A difference in the beam spectrum means that the number of high energy photons per equivalent quantum depends upon the crystal rotational position. Note that such an error can arise from an asymmetry in the low energy portion of the spectrum as well as the high energy portion, since the former is included in the measurement of the total number of equivalent quanta.[15] With such differences the error in the measured asymmetry is given by

$$\Sigma_m - \Sigma P = \Lambda\left(1 - \Sigma^2 P^2\right) - p\Sigma^2 P^2 \quad , \tag{10}$$

where Λ is the asymmetry of the beam spectrum,

$$\Lambda(k) = \frac{\lambda_\perp(k) - \lambda_\parallel(k)}{\lambda_\perp(k) + \lambda_\parallel(k)} \quad , \tag{11}$$

where $\lambda_\perp$ ($\lambda_\parallel$) is the beam spectrum normalized per equivalent quantum when the polarization is perpendicular (parallel) to the scattering plane, and p is the asymmetry in the polarization

$$p = \frac{p_\perp - p_\parallel}{p_\perp + p_\parallel} \quad . \tag{12}$$

In general, the causes of asymmetries in the polarization are the same as those in the spectrum. Because the errors due to the asymmetry in the polarization are suppressed by the factor $\Sigma^2 P^2$ in Eq. (10), the asymmetries in the beam spectrum dominate the error and consequently set the necessary tolerances.

The sweeping magnet bent the pairs in the vertical plane independent of the crystal rotation. If in rotating the crystals the pairs were swept through different amounts of material (due to the non-symmetric design of the surrounding crystal holders and assembly), and if the resulting bremsstrahlung photons from these pairs remained in the beam, the beam spectrum would be asymmetric. To remove this source of asymmetry the beam was collimated upstream of the crystals to insure that the photons struck only the graphite, and downstream to insure that any secondary photons came from an area in the graphite defined by the fixed collimator. After consideration of the electron beam spot size and the divergence of the photon beam, the collimator sizes were chosen to be 6.1×6.1 mm upstream and 6.35×6.35 mm downstream of the 9.5 mm square crystals.

The shape of the beam spectrum is determined by the tilt angle θ, which changes when the crystals are rotated if the rotation axis is not parallel to the beam. The attenuation function $A(k, \theta)$ (as will be defined by Eq. (15)) of the crystals is shown as a function of θ for k = 15 and 16 GeV in Fig. 6a. In the region of optimum polarization between 8 and 12 mrad (see Fig. 6b) the magnitude of the derivative $dA/d\theta$ is less than 10^{-2} mrad^{-1}. In order that the error thus introduced into the asymmetry be small compared to the statistical error $\delta \Sigma_m$ of the measured asymmetry, we then require

$$|\Lambda| \simeq \left| (\theta_\perp - \theta_{||}) \frac{dA}{d\theta} \right| / 2A \ll \delta \Sigma_m \qquad (13)$$

or

$$|\theta_{\perp} - \theta_{\parallel}| \ll 2 \text{ mrad} \tag{14}$$

for the desired statistical error of $\delta\sum_m \sim 2\%$. The tolerance for the alignment of the rotation axis with respect to the beam was set to ± 0.3 mrad in both the horizontal and vertical projections.

The error in the relative alignment of the crystals should be small compared to their mosaic spread. This tolerance (including errors in the alignment of gauge surfaces with respect to the crystal planes) was placed at ± 1 mrad on each crystal.

4. Device description

A. The crystal assembly

Figure 7 is an assembly drawing of the polarizer-analyzer, and Fig. 8 and 9 show photographs of the device. Details of a single crystal subassembly are shown in Fig. 10. The device consisted of two independent and functionally identical assemblies (polarizer and analyzer). For each assembly there were three possible motions: in and out of the beam, 90° rotation about the beam, and tilt of the crystal planes relative to the beam.

The in-out motion was accomplished by simultaneously driving three 1.00-in by 0.25-in lead ball screws with a 100-step-per-revolution, 400-oz-in torque, radiation-resistant motor.

The 90° rotation was accomplished by rotating the entire C-shaped assembly containing the crystal subassemblies. This frame was constructed out of 2024 aluminum for easy machining and dimensional stability. Each end of the C-frame was mounted in a 4.0-in bearing chosen for its small width and good angular tolerances. In the machining of the C-frame all critical dimensions were measured

from the axis defined by the two bearing centers, and the tooling balls (used in aligning the device in the beam line) mounted on the bulkheads were measured relative to the bearing axis. An air cylinder drive system rotated the C-frame to and maintained pressure against one of two positive stops. There was no provision for the crystals' being in other than one of these two positions. The stops were positioned to correspond to the reciprocal lattice vectors' being horizontal or vertical within $\pm 0.25^{o}$.

To understand the method by which the crystal axes were oriented relative to the beam, we must first describe in greater detail the individual crystal sub-assemblies as shown in Fig. 10. Each crystal was in a water-cooled 5086 aluminum cart. The bottom of the slot containing the graphite was machined parallel and perpendicular to within $\pm$ 0.6 mrad to the two external surfaces (referred to below as the gauge surfaces). This crucial step in the machining was done after all heli-arcing and other operations which might distort the carts. Because of the natural cleavage of the graphite, the crystal face mounted against the bottom of the slot was one of the crystal planes, and, therefore, the gauge surfaces of the cart were parallel and perpendicular to the crystal planes. The mounting of the crystals in the carts was done by Union Carbide at their Parma Technical Center.

The carts were mounted in the C-frame with a three-point support. Two of the points were the rounded end of a differential screw (with leads of 0.03125 in and 0.02777 in, allowing a motion of 0.00348 in per revolution) which fit into a radius cut in the bottom of the cart. These two points formed a pivot about which the carts could rotate. The third point of the support was a small ball bearing mounted similarly to the wheel of a wheel-barrow. This mounting consisted of differential screws of the same pitch as those used for the pivots. The ball bearing rested on a saw-tooth cam to be described below. The carts were held down

on the pivots and the bearing on the cam by three ball-nosed spring plungers, each exerting approximately six pounds of force.

The mounting of the carts was the only serious design flaw of the crystal assembly. Wear in the pivot sockets and at the points where the spring plungers exerted pressure caused the behavior of the pivots to deviate from that of true pivots. Fortunately, the problem was discovered before installation in the beam, and the pivot sockets were replaced with anodized sockets and the pressure points were reinforced with tool steel. Although not a permanent solution, it was an adequate temporary one. A captive pivot is contemplated as a permanent solution.

By moving the saw-tooth cam along the C-frame length, the elevations of the ball bearings were changed, and the carts rotated about the pivots. This tilted the crystals with respect to the beam, giving adjustment of the angle θ of Fig. 5. The saw-tooth cam was constructed from stainless steel segments brazed onto a flat 9.1×4.6 mm stainless steel bar. A single stainless steel piece was ground to the correct angle and separated into segments, thus insuring that all segments of the cam had the same angle. This angle was 25.0 mrad, giving a crystal change of 6.12 mrad per cm of cam motion. The segments, along with a water-cooling tube, were tack-welded and then brazed onto the stainless steel bar with a slow brazing process. While some warpage of the bar occurred during the tack-welding, it was easily straightened before brazing.

With the cam held in a fixed position, the carts were installed in the C-frame and aligned using the gauge surfaces, a granite surface table, and mechanical feeler gauges. All carts were aligned to the same angle within $\pm$ 0.8 mrad. This alignment was performed with the water hoses in place in order to have all of the forces which would be present during use acting on the carts during alignment.

The cam drive system is shown in Fig. 11. The cam was held captive to a block by ball bearings. The block and cam assembly was moved by a 26.5° wedge

mounted on a 0.625-in by 0.200-in lead ball screw driven by a 100-step-per-revolution, 50-oz-in torque, radiation-resistant motor through a 21.66:1 planary gear assembly. During the 90^{o} rotation the cam rotated with the C-frame, while the block and wedge assembly remained fixed.

B. The control system

All functions of the device were remotely controllable, and careful interlocking was provided to guard against catastrophic damage by the beam. Additionally, automatic sequencing was provided for several functions for which the interlock system required a prescribed sequence of events. The complete status and positioning of the device could be read and displayed by the online computer used in the experiment. The 90^{o} rotation, which was the most frequently exercised function, could be controlled either manually or through the computer.

As long as the device was installed in the beam, the interlock system suppressed the beam unless the electron beam dump magnets were powered, thus preventing the high power electron beam (rather than the lower power photon beam) from reaching the polarizer. The photon beam was further interlocked to flow switches and temperature monitors on the collimator and crystal subassembly water-cooling systems, and to the sweeping magnet current. The latter interlock prevented full beam from being delivered to the crystals unless the sweeping magnet was at full current. The beam was further suppressed unless both crystal assemblies were clearly out of or centered on the beam line.

An extensive array of thermocouples was mounted at various points on the assembly in order to detect any heating problems which might arise. These could be read by computer or experimenter through a digital voltmeter, but were not part of the interlock system.

The nominal in-out positions of the polarizer and analyzer assemblies were sensed with microswitches. The precise in-beam position of each assembly was

determined by a continuous single-turn potentiometer mounted on one of the ball screws. To position the assembly in the beam, the beam was first suppressed to prevent its striking and damaging the crystal holder. The assembly was then driven into the beam until the in-position microswitch was reached, at which time the beam permissive was restored. The crystal assembly was then driven further into the beam until the reading of the potentiometer matched that determined when the assembly was surveyed into the beam line.

The two 90° rotation states were sensed by microswitches mounted on the drive mechanism. To change polarization the following sequence occurred: the beam was first-limited to one pulse per second (rather than the nominal 180) in order to maintain control of the beam without overheating the crystals when the sweeping magnet current was lowered; the sweeping magnet current was then lowered to a very small value to prevent eddy current resistance to the rotation; the crystal assembly was then rotated, the sweeping magnet restored to full current, and the beam returned to full repetition rate. A 90° rotation required approximately 30 seconds to complete.

The tilt angle of the crystals was monitored by counting the number of pulses applied to the stepping motor, and by a high precision linear potentiometer mounted on the block which drove the cam. The desired position could be preset onto a set of thumbwheels, and a button pushed to start the motor driving to that point.

5. Experimental studies

The properties of the polarized photon beam were studied during two test runs at SLAC. The objectives of the tests were to choose a suitable angle of the crystals relative to the beam direction, to measure the polarization of the beam, to measure the energy spectrum of the beam, and to check for possible beam spectrum asymmetries between the two rotational positions of the crystals. In this

section we present the rationale and method for each of the measurements, and in Section 6 we present the analysis and results.

A. Pair spectrometer measurements

In single arm spectrometer experiments with a continuous incident beam spectrum, a knowledge of the beam energy spectrum is necessary even for asymmetry (rather than cross section) measurements in order to disentangle several possible reactions (e.g., $\gamma p \rightarrow \pi^+ n$, $\gamma p \rightarrow \pi^+ \Delta^o$, $\gamma p \rightarrow \pi^+ +$ multi-particles, etc.). Using the SLAC pair spectrometer,[16] energy spectra were measured for both the polarizer and analyzer separately and with both sets of crystals removed from the beam (ordinary bremsstrahlung). The measured spectrum of the polarizer was divided by that from the amorphous radiator alone to obtain the attenuation function A(k) such that the energy spectrum dn(k)/dk of the polarized beam is given by

$$dn(k)/dk = A(k)\, B(k, E_0)/k \tag{15}$$

where $B(k, E_0)$ is the bremsstrahlung function of the incident beam, and E_0 (= 16.05 GeV) is the end point energy of the spectrum. While in principle dn(k)/dk is directly measurable, without measuring the ordinary bremsstrahlung spectrum, the quantity $B(k, E_0)$ is easily calculated,[17] and the crystal spectrum was therefore normalized to the ordinary spectrum in order to eliminate systematic biases in the pair spectrometer.

By measuring the spectrum of the polarizer (and, separately, the analyzer) in both rotational positions, one could directly check for experimental asymmetries in the beam spectrum.

To measure the absolute value of the beam polarization, two independent crystal assemblies were used as a polarizer-analyzer pair and the transmitted intensity measured with the pair spectrometer. By measuring the transmitted beam

intensity with the direction of beam polarization of the analyzer parallel (aligned) and perpendicular (crossed) to that of the polarizer, one could obtain the asymmetry

$$\epsilon(k) = \frac{I_a(k) - I_c(k)}{I_a(k) + I_c(k)} = P_p(k)\, P_a(k) = P_p(k)^2/R(k) \ , \qquad (16)$$

where I_a (I_c) is the transmitted beam intensity with the polarizer-analyzer aligned (crossed), P_p (P_a) is the polarizing power of the polarizer (analyzer) as given by Eq. (7), and $R = P_p/P_a$ is the ratio of the polarizing power of the polarizer to that of the analyzer.

An argon-CO_2 filled quantameter[18] was used to monitor the beam during the spectrum measurements. The quantameter was not a suitable monitor for the aligned/crossed asymmetry measurements, since the shape of the spectrum depends upon whether the two assemblies are crossed or aligned. The quantameter measures the total energy of the beam, whereas one wishes to measure the total number of transmitted photons per incident photon at a given energy. Consequently we used transmitted photons at a lower energy (which have a negligible aligned/crossed asymmetry) as the beam monitor. To accomplish this a second (1.4% radiation length copper) converter was placed 18 inches from the downstream end of the 72-in long pair spectrometer magnet (see Fig. 12). Electron-positron pairs created in the second converter traversed only $\sim$ 25% of the total magnetic field; thus the detectors were sensitive to photons of $\sim$ 4 GeV. These pairs were easily distinguished from the 16 GeV pairs created in the upstream converter on the basis of shower counter pulse height and track extrapolation.

B. 20-GeV spectrometer measurements

Assuming a polarization $P_p \simeq .25$ and $R = 2$ in Eq. (16), one expects an asymmetry $\epsilon \simeq 0.03$ using the polarizer-analyzer technique. The small size of this asymmetry made it prohibitive to use such a method to optimize the tilt angle of

the crystals. Since this optimization required only relative asymmetry measurements, it could be made using any reaction having a large asymmetry. From lower energy measurements of single π^+ photoproduction, the asymmetry in that reaction was expected to be large, and therefore could be used as an analyzer. Using the SLAC 20-GeV spectrometer[19] to measure the asymmetry in π^+ photoproduction as given by Eq. (4), we could therefore measure the relative beam polarization for different orientations of the crystals. By using the "analyzer" as polarizer, we could also measure the polarizing power of the analyzer relative to that of the polarizer (i.e., the parameter R of Eq. (16)).

On the basis of the calculated beam properties the tilt angle of the crystals was chosen to be 10.5 mrad to maximize the beam polarization between 15 and 16 GeV. Detailed asymmetry measurements to verify the curves of Fig. 6b with reasonable precision would have required large amounts of running time. Additionally, because of the previously mentioned problem with the pivot points, we were reluctant to change the tilt angle of the crystals more than was absolutely necessary. Consequently, detailed studies were not done, but sufficient measurements were taken at different angles and at a lower energy (15 GeV) to establish that the beam behaved in qualitative accord with expectations. Because of the large mosaic spread of the crystals, none of the important beam parameters are exceptionally sensitive to the crystal angle, so that more quantitative measurements were not necessary.

As mentioned earlier, the flux of lower energy photons through the analyzer-polarizer was used as the beam monitor during the pair spectrometer measurement of the beam polarization. This relies on the assumption that the beam polarization at 4 GeV is small compared to that at 16 GeV, which was verified by lowering the energy of the electron beam to 4 GeV and measuring π^+ photoproduction at this energy.

C. Experimental setup

A schematic of the experimental setup is shown in Fig. 13. The SLAC electron beam was passed through a 2.85% radiation length aluminum radiator to produce an unpolarized bremsstrahlung beam. The electrons were then bent out of the beam by bending magnets and the remaining photon beam passed through the graphite polarizer and/or analyzer. Electron-positron pairs created in the graphite were swept out by the bending magnet (a C-magnet 36 inches long with a gap 6 inches wide by 9 inches high and run at 10 kG) surrounding the crystal assembly. The beam was collimated immediately upstream and at three points downstream of the polarizer (the latter two followed by sweeping magnets). The upstream collimator was split into two sections and an air-filled ion chamber was placed between them. The ion chamber had a hole along the beam axis so the beam could be properly steered by minimizing the ion chamber signal.

During the 20-GeV spectrometer running, the spectrometer, which was placed at 1.4° relative to the beam direction, detected positive pions photoproduced in a 1-meter long liquid hydrogen target. The beam was monitored upstream of the target by a gas Cerenkov monitor[20] and two ion chambers, and downstream by a secondary emission quantameter (SEQ)[20] which also served as a beam dump.

During the pair spectrometer running, the hydrogen target and SEQ were removed from the beam, the 20-GeV spectrometer was moved to a larger angle, and the pair spectrometer and associated sweeping magnet were placed directly in the beam. The beam was monitored by an argon-CO_2 filled quantameter[18] placed immediately behind the pair spectrometer.

D. Experimental running

During the first test run the 20-GeV spectrometer was used to measure the relative beam polarization at 16 GeV for several crystal angles. Spectra for the unpolarized beam and for the polarizer and analyzer were measured with the pair spectrometer. An attempt to measure the absolute polarization of the beam was

marred by difficulty in obtaining a sufficiently stable low-intensity beam necessary for precision pair spectrometer measurements.

A heating problem in the saw-tooth cam was also discovered during the first test run. Between the two test runs, the entire crystal assembly was removed from the beam line and disassembled. Water cooling was installed on the cam, and the crystal assembly was then reassembled, realigned, and reinstalled in the beam.

During the second test run the 20-GeV spectrometer was first used to verify that the results of the first run could be reproduced. The relative asymmetries for polarizer and analyzer were measured at 15 and 16 GeV with the crystal tilt angle set at 10.5 mrad. A scheme for obtaining a stable low-intensity beam was devised and the absolute polarization of the beam measured. The spectra for the ordinary and polarized beams were remeasured.

Following the second test run, the polarized beam was used continuously for a period of four weeks in an experiment to study pseudoscalar meson photoproduction. During this run the check at 4 GeV was made. Typical intensities of 1×10^{10} equivalent quanta per pulse incident on the crystals resulted in intensities of $\sim 4\times 10^{8}$ equivalent quanta per pulse in the attenuated beam. The number of photons near the endpoint of the beam was further suppressed relative to an ordinary bremsstrahlung beam by a factor of approximately 2 by the attenuation function A(k) in Eq. (15).

During the experiment several of the non-critical mechanical and electrical functions of the controller failed due to radiation damage or water damage (which occurred as a result of the bursting on several occasions of radiation-damaged water hoses on the sweeping magnet). At several points during the experiment the asymmetry measurement at 1.4° was repeated. These measurements showed that the polarization remained constant to within $\pm$ 0.008, indicating no evidence for deterioration in the polarizing power of the crystals.

6. Analysis and results

A. 20-GeV spectrometer measurements

Analysis of π^+ photoproduction data using the SLAC 20-GeV spectrometer has been discussed elsewhere,[21] and we describe here only those points relevant to the asymmetry measurements. A typical cross-section spectrum obtained with the spectrometer at a fixed central momentum is shown in Fig. 14a as a function of π^+ momentum. The spectrum at the highest momenta mirrors the incident beam spectrum. The rise in the spectrum at lower momenta is due chiefly to a similar effect for the reaction $\gamma p \longrightarrow \pi^+ \Delta^0$.

By measuring the cross-section spectra with the beam polarization parallel and perpendicular to the horizontal plane of scattering, one could form the asymmetry spectrum as given by Eq. (4) and shown in Fig. 14b. The drop in the asymmetry at lower momenta is again due to the process $\gamma p - \pi^+ \Delta^0$, which has a smaller asymmetry than does $\gamma p \longrightarrow \pi^+ n$.

A simultaneous fit was done to the cross section and asymmetry spectra to obtain the cross section and asymmetry for the $\pi^+ n$ reaction. The fitting program took into account the incident beam spectrum, spectrometer resolution, polar angle dependence of the cross section, and azimuthal angle dependence of the asymmetry.

The statistical errors on the measurements of the asymmetry at the different crystal tilt angles were sufficient only to qualitatively verify that the asymmetry was at or near maximum with the crystal tilt angle set to the calculated value of 10.5 mrad. With the crystals set to the final operating value of 10.5 mrad, asymmetries of 0.1903 ± 0.0073 and 0.2030 ± 0.0088 were measured at 15 and 16 GeV respectively, verifying that the asymmetry did not change rapidly as a function of energy. At both 15 and 16 GeV a value of $R = 1.80 \pm 0.11$ was

obtained for the ratio of polarizer to analyzer polarizing power. This should be compared to an expected value of 1.97 for an analyzer of one-half the length of the polarizer, and will be discussed later in conjunction with the pair spectrometer measurements.

With a beam energy of 4 GeV an asymmetry of 0.019 ± 0.013 was measured. Assuming that the analyzing power of the photoproduction process is the same at both energies (which is correct to within the accuracy needed here), one obtains a ratio of 0.094 ± 0.065 for the polarization of 4 vs 16 GeV photons, consistent with the expected ratio. This introduces a negligible error of 0.001 into the final measurement of the beam polarization.

B. Pair spectrometer measurements

The analysis of the spectrum measurements (but not the asymmetry measurements) using the pair spectrometer was done in the same manner as has been described elsewhere.[16] Figure 15 shows the spectra obtained for (a) an unpolarized bremsstrahlung beam, (b) a bremsstrahlung beam attenuated by the analyzer, (c) a bremsstrahlung beam attenuated by the polarizer, and (d) a bremsstrahlung beam attenuated by both analyzer and polarizer.

A four-parameter fit to the ordinary bremsstrahlung spectrum is shown in Fig. 15a. The fit uses the bremsstrahlung function calculated for a 2.85% radiation length aluminum radiator[17] and includes the effect of radiative straggling of the electron and positron in the 4.4% radiation length copper converter of the pair spectrometer. The four parameters of the fit are (1) an overall normalization factor (which should = 1.0), (2) the finite resolution of the pair spectrometer (calculated to be 0.75%) from considerations of multiple coulomb scattering and the finite size of the hodoscope counters, (3) an offset in the end point energy (which should = 0), and (4) a one-parameter calculation of the accidentals spectrum (which accounts for the non-zero spectrum beyond the end point energy).

The resulting fit to the data is rather poor. The data below the end point show a slope not present in the calculated spectrum, and the fit requires an offset in the end point energy of 0.10 out of 16.05 GeV. These discrepancies are believed to be due to an inexact accounting taken of the alignment of the hodoscopes and magnet, as measured in a survey before the experiment. The analysis programs are not at present capable of handling some of the observed geometrical differences between the two spectrometer arms, and work is in progress to account for these effects.

A fit to the spectra from 14 to 16 GeV, where the efficiencies are not critically dependent on geometry, gave values for the normalization constant of 0.977 ± 0.017 and 1.008 ± 0.009 for the data taken during the first and second test runs, respectively. (Fitting the entire spectrum gave results 1.4% higher.) This gives fair agreement between the two sets of data, and the agreement with the expected value is well within the estimated 4% normalization error of the experiment due to quantameter calibration, quantameter drift current, electronics dead-time, and hodoscope corrections.

To avoid the problem mentioned above in measuring the exact shape of the spectra, the attenuation function A(k) of Eq. (15) was obtained by dividing the attenuated spectrum by the unattenuated spectrum on a point-by-point basis. The attenuation function obtained for the polarizer is shown in Fig. 16. A three-parameter fit was made to the data on the basis of the calculated shape of the attenuated spectrum. The three parameters were a normalization constant and two terms to account for the accidentals in the attenuated and unattenuated spectra. The resulting curves for both the polarizer and analyzer (that for the polarizer is shown in Fig. 16) gave good fits to the data. The normalization constants obtained were $\simeq$ 10% lower than those obtained by calculation alone. This, however, is to

be expected since the calculations did not include the effect of secondary processes in the crystal. These contribute predominantly to the low energy portion of the spectrum and consequently suppress the number of high energy photons per equivalent quantum. Good agreement was found between the attenuation functions obtained during the first and second test runs.

To look for experimental asymmetries between the two rotational positions of the crystals, we have calculated the asymmetry (summed over the energy acceptance of the spectrometer) between the two rotational states for the different analyzer and/or polarizer configurations. The results are summarized in Table I. The data show no statistically significant evidence for asymmetries between the parallel and perpendicular configurations.

C. Pair spectrometer asymmetry measurements

The treatment of the crossed vs aligned asymmetry measurements differed from that of the spectrum measurements in several respects. As mentioned previously, low energy electron-positron pairs from a downstream converter were used as the beam monitor to guard against differences in spectrum shapes. The spectrum measurements were designed to measure absolute rates, whereas the asymmetry measurements could ignore effects which cancelled in forming the asymmetry. On the other hand, effects of less than 1% were relatively unimportant for the spectrum measurements but very important for the asymmetry measurements, since the total asymmetry was only $\simeq$ 3%. In particular, care was taken to eliminate rate dependent effects since the very low intensity beam was difficult for the accelerator operators to monitor, leading to large short-term intensity fluctuations.

The fast electronics logic was designed to equalize the dead times for triggers due to high or low energy photons. High or low energy events were equally

likely to have spurious tracks which could contribute to the shower counter pulse heights and thus bias the event toward high energy interpretation; therefore all events with multiple tracks in the hodoscopes (which in most cases could be salvaged in the spectrum measurements) were rejected.

For each event with clean hodoscope tracks the positron and electron tracks were extrapolated to their apparent point of intersection, and the coordinates x, y, and z were obtained for the horizontal, vertical, and longitudinal positions, respectively, of the intersection point. All valid events were required to satisfy cuts placed on the x and y positions, and agreement was also required between the x positions determined from each arm separately. Separate cuts appropriate to high or low energy photons were applied to the shower counter pulse heights and to the z coordinate of the intersection point. The separation between high and low energy events is shown in Fig. 17. Events satisfying all low energy cuts were simply counted and used as a relative beam monitor. An energy distribution for each of the four possible configurations of the two sets of crystals was formed from the valid high energy events, from which one could form an asymmetry spectrum as given by Eq. (16).

A set of runs was also made at higher than normal beam intensities. From these data a definite rate dependence was observed in the ratio of high energy to low energy events, due to pile-up in the shower counter pulse heights and accidental coincidences in which the electron and positron originated from different photons.

Accidental coincidences could be easily monitored by observing the number of events in which the electron originated from one converter and the positron originated from the other. From the high and low energy counting rates in the single arms one could then calculate the accidental rates for events coming from

the same converter. The results of such calculations were in reasonable agreement with those obtained from accidental circuits in the fast electronics and from the number of high energy events beyond the end point of the spectrum. Because the accidental rates from the two converters were comparable, they tended to cancel in the ratio of high to low energy events and consequently contributed a relatively small amount to the rate dependence.

To study the rate dependence due to pulse height pile-up in the shower counters, the shower counter pulse height distributions were studied using the z coordinates obtained from track extrapolation. Because the beam spot size was sufficiently small, a z-position for each arm could be obtained by extrapolating to the beam line rather than to the point of intersection. While the distributions thus obtained showed some overlap between the two converters, an unambiguous sample could be obtained by rejecting events which fell within the ambiguous region. By studying the shower counter distributions for the unambiguous events, an estimate could be made for the number of low energy events which had been rejected on the basis of pulse height, although for some effects this was an upper limit rather than a reliable estimate. The rate dependence thus obtained (including the use of the upper limits) was in good agreement with the observed rate dependence.

The beam intensities for the data actually used to measure the polarization covered a sufficiently small range that no rate dependence could be seen in that data alone. The rate dependence correction varied by 3% over the range of intensities for these data. Furthermore, because the crystals were rotated frequently ($\sim$ every ten minutes), changes in beam intensity tended to average out. When all the data were combined in the analysis, the crossed and aligned data proved to be very well matched in beam intensity in that the overall accidental rates for the two sets of data were the same to within statistical counting errors ($\simeq 0.05\%$).

Approximately 40 runs were taken for each of the four rotational configurations. The ratio of the number of high energy to low energy events (suitably rate corrected) for each configuration was checked for run-to-run consistency, and gave confidence levels for agreement which ranged from 15% to 50%, indicating that some run-to-run fluctuations were present in addition to the normal statistical fluctuations in the counting rates. To account for this the errors assigned to the results were enlarged by 6% of themselves to obtain a chi-square of 1 per degree of freedom in fitting the four sets of data to two constants. Fitting the data to four rather than two constants did not significantly improve the fit.

To obtain the final value of the beam polarization, the aligned vs crossed asymmetry data were fit using the calculated shape of the polarization as a function of energy, allowing a free normalization constant. The fitted results are shown in Fig. 18 and give only an 8% confidence level ($\chi^2 = 33$ for 23 degrees of freedom). The data could be checked for systematic errors by forming the asymmetry between the two sets of aligned and between the two sets of crossed data. The results, summed over the energy acceptance of the pair spectrometer, are shown in Table II, and are consistent with the expected value of 0. Chi-squares for agreement of the individual points with the average are comparable to that obtained in the fit to the aligned vs crossed asymmetry data, and indicate the presence of some systematic errors in the data comparable to but smaller than the statistical uncertainty in the data. Examination of the data failed to reveal any systematic shape dependence or energy region giving rise to the larger than expected chi-square. When combined with the statistical uncertainty in the beam normalization and the ratio of polarizer to analyzer polarizing power (R of Eq. (16)), this point-to-point systematic error introduces a negligible enlargement in the uncertainty in the net beam polarization.

The value of the beam polarization extracted from the fit depends upon the value assumed for R in Eq. (16). As mentioned previously, the value of R obtained

from the 20-GeV spectrometer measurements was (averaging the 15 and 16 GeV results) 1.80 ± 0.08, which should be compared with an expected value of 1.97. However, this number is sensitive to very small false asymmetries in the beam spectrum (particularly for the analyzer). Using the measured values of the asymmetries in the beam spectrum between parallel and perpendicular orientations, as given by Table I, we obtain a corrected value of R of 1.97 ± 0.15. Note that the corrected value of R is consistent with the uncorrected value. We feel that the enlargement in the uncertainty thus obtained is more significant than the change in the value itself.

Using this value of R, one then obtains a value of 0.255 ± 0.020 for the beam polarization, where the error includes the statistical error in the asymmetry measurement (enlarged by 6% as previously mentioned) and the statistical error in R, including the error arising from the uncertainty in the beam spectrum asymmetry.

7. Summary and conclusions

We have polarized a bremsstrahlung beam by using coherent pair production in graphite crystals. The polarization of the beam over the last GeV of the spectrum has been measured to be 0.255 ± 0.020. We have also measured the beam spectrum and established that it has no significant false asymmetry.

The unique advantage of this beam is the combination of high intensity and polarization of the highest energy portion of the beam spectrum. The beam has been used to study several pseudoscalar meson photoproduction reactions. These studies would not have been possible with beams polarized by other techniques.

At higher energies coherent pair production becomes a more effective polarizer. Therefore this type of beam should play an important role in future photoproduction studies.

8. Acknowledgments

We would like to mention and thank the many people who have contributed to the success of this project. D. Coward and B. Richter have supported and shown considerable interest in this work. D. Gustavson and R. Talman introduced us to coherent pair production and have shared their knowledge of the subject. R. Schwitters has provided both many insights into coherent processes and the computer program used for the calculations. A. Moore of Union Carbide Corporation has been a valuable source of information about graphite crystals.

B. Humphrey and M. Browne designed and tested the control system. S. Dyer, L. Boyer, and A. Filippi provided much of the technical support needed throughout the project. E. Taylor, A. Golde and the crew working in End Station A prepared and maintained the spectrometers during the experiment. Finally we are indebted to the SLAC operations staff for providing useful beams ranging over eight orders of magnitude in intensity.

References and footnotes

1. Most pseudoscalar meson photoproduction processes fall into this category. At 16 GeV, the cross section for $\gamma p \longrightarrow \pi^+ n$ is less than 0.1% of the total cross section.
2. G. Diambrini Palazzi, Rev. Mod. Phys. 40, 611 (1968).
3. R. L. Anderson, D. Gustavson, J. Johnson, I. Overman, D. Ritson, B. H. Wiik, R. Talman, and D. Worcester, Phys. Rev. Letters 26, 30 (1971).
4. R. F. Schwitters, J. Leong, D. Luckey, L. S. Osborne, A. M. Boyarski, S. D. Ecklund, R. Siemann, and B. Richter, Phys. Rev. Letters 27, 120 (1971).
5. N. Cabibbo, G. Da Prato, G. De Franceschi, and U. Mosco, Phys. Rev. Letters 9, 270 (1962); N. Cabibbo et al., N. Cim. 27, 979 (1963).
6. C. Berger, G. McClellan, N. Mistry, H. Ogren, B. Sandler, J. Swartz, P. Walstrom, R. L. Anderson, D. Gustavson, J. Johnson, I. Overman, R. Talman, B. H. Wiik, D. Worcester, and A. Moore, Phys. Rev. Letters 25, 1366 (1970).
7. D. J. Sherden, R. H. Siemann, C. K. Sinclair, D. J. Quinn, J. P. Rutherfoord, and M. A. Shupe, SLAC-PUB-1206 (to be published).
8. A. W. Moore, A. R. Ubbelohde, and D. A. Young, Nature (London) 198, 1192 (1963); A. W. Moore et al., Proc. Royal Soc., Ser. A280, 153 (1964); the crystals are graphite monochromators, grade ZYA, purchased from Union Carbide Corporation, Parma, Ohio.
9. N. F. Graves, A. W. Moore, and S. L. Strong, in Proceedings of the Ninth Biennial Conference on Carbon, Boston, Mass., June 1969, Abstract CA-27.
10. G. E. Bacon, Nature (London) 166, 794 (1950).
11. D. Cramer and J. Waber, Acta Crystallogr. 18, 104 (1965).
12. L. C. Montgomery, private communication. Measurements were made on areas $\simeq 1 \times 5$ mm, using Cu K_α radiation of 1.5 Å wavelength.

13. Typically, mosaic spreads as measured by neutron diffraction (volume sensitive) are $\sim$ 2 mrad greater than those measured by x-ray diffraction (area sensitive). A. W. Moore, private communication.

14. D. Gustavson and R. F. Schwitters, private communication.

15. All spectra are normalized per equivalent quantum, i.e., $\int k\, dn(k)/dk\, dk = E_0$. This unit is useful since total absorption monitors (such as the quantameter and SEQ used in this experiment) measure the total energy of the beam, which is then equal to the total number of equivalent quanta divided by the beam end-point energy, independent of the shape of the beam spectrum.

16. SLAC Users Handbook, p. D.3-7 (1971, unpublished); A. M. Boyarski, D. H. Coward, S. Ecklund, B. Richter, D. Sherden, R. Siemann, and C. Sinclair, Phys. Rev. Letters 26, 1600 (1971).

17. R. A. Early, SLAC-TN-66-15 (1966, unpublished).

18. D. Yount, Nucl. Inst. and Meth. 52, 1 (1967).

19. SLAC Users Handbook, p. D.3-5 (1971, unpublished).

20. G. E. Fischer and Y. Murata, Nucl. Inst. and Meth. 78, 25 (1970).

21. B. Richter, Proc. 1967 Int. Symp. on Electron and Photon Interactions at High Energies, p. 309-336 (1968).

List of Tables

I. Measured asymmetries in the beam spectra per equivalent quantum, summed over the energy acceptance of the spectrometer. The orientations refer to the polarization direction relative to the horizontal plane. For the case of both analyzer and polarizer in the beam, the first orientation symbol refers to the polarizer and the second to the analyzer. The chi-squares refer to the agreement of the individual points (i.e., in a single energy bin) with the average.

II. Measured asymmetries between crossed or aligned spectra per transmitted 4-GeV photon, summed over the energy acceptance of the spectrometer. Orientation symbols and chi-squares have the same meaning as for Table I.

Table I

Attenuator	Orientation	Asymmetry	χ^2/d. f.
polarizer	$\frac{\perp - \parallel}{\perp + \parallel}$	-0.0011 ± 0.0058	25/25
analyzer	$\frac{\perp - \parallel}{\perp + \parallel}$	0.0085 ± 0.0055	37/25
polarizer and analyzer	$\frac{\perp\perp - \parallel\parallel}{\perp\perp + \parallel\parallel}$	0.0006 ± 0.0031	32/25
polarizer and analyzer	$\frac{\perp\parallel - \parallel\perp}{\perp\parallel + \parallel\perp}$	-0.0034 ± 0.0032	36/25

Table II

Orientation	Asymmetry	χ^2/d. f.
$\frac{\perp\perp - \parallel\parallel}{\perp\perp + \parallel\parallel}$	0.0038 ± 0.0042	44/25
$\frac{\perp\parallel - \parallel\perp}{\perp\parallel + \parallel\perp}$	-0.0041 ± 0.0042	24/25

Figure Captions

1. A measured coherent bremsstrahlung spectrum from a diamond radiator. See Ref. 4 for an explanation of the curves.
2. The pair production cross sections as a function of the energy partition for photons with polarization vectors perpendicular and parallel to the normal to the crystal planes. The discontinuities occur when a reciprocal lattice vector no longer satisfies the kinematic condition (Eq. (1)) for pair production.
3. The pair production cross sections as a function of the angle θ between the normal to the crystal planes and the normal to the photon direction.
4. The pair production cross section times the distribution in θ (see text) integrated over θ; (a) as a function of photon energy for the central value of the θ distribution equal to 10.5 mrad; (b) as a function of the central value of the distribution for photon energy equal to 16 GeV.
5. The necessary motions of the crystal. To change the direction of the beam polarization vector, the crystal is rotated 90° about the beam line, and to change the energy at which the photons have greatest polarization, the angle θ is changed. The net beam polarization is in the plane defined by the beam axis and the reciprocal lattice vectors of the crystals.
6. (a) The attenuation function (Eq.(15)), and (b) the beam polarization as a function of the angle θ for 15 and 16 GeV photons.
7. Drawing of the crystal assembly showing side and top views.
8. Photograph of the crystal assembly.
9. Photograph of the crystal assembly showing the analyzer in detail.
10. Drawing of a single crystal subassembly.

11. Schematic of the cam drive system. The saw-tooth cam is captured to the block by ball bearings on each side of the block. During the 90^{o} rotation these bearings roll along the faces of the block.

12. Schematic of the pair spectrometer showing the two converters for high and low energy photons.

13. Schematic of the experimental set-up showing the pair spectrometer in position. During the 20-GeV spectrometer running the pair spectrometer was removed from the beam line and the SEQ placed in the beam line upstream of the 20-GeV spectrometer.

14. (a) Cross section, and (b) asymmetry spectra obtained with the 20-GeV spectrometer. The spectra at high momenta are dominated by $\gamma p \longrightarrow \pi^{+} n$, and at lower momenta by $\gamma p \longrightarrow \pi^{+} \Delta^{o}$. The curves are from a 6-parameter fit to the data, as described in the text.

15. Beam spectra measured with the pair spectrometer; (a) ordinary bremsstrahlung, (b) attenuated by analyzer, (c) attenuated by polarizer, (d) attenuated by analyzer and polarizer. The curve in (a) is from a 4-parameter fit to the data as described in the text.

16. Measured attenuation function A(k), as defined by Eq. (15) of the text, of the polarizer. The dashed curve is from a calculation with no free parameters and the solid curve is a fit to the data allowing an arbitrary normalization.

17. Isometric display of the number of events as a function of shower counter pulse height (proportional to pair energy) vs longitudinal position of the intersection point of the extrapolated tracks. The separation of events from the two converters is clearly seen.

18. The polarizer-analyzer aligned vs crossed asymmetry spectrum measured with the pair spectrometer. The asymmetry is the product of the polarizing powers of the polarizer and analyzer. The dashed curve is from a calculation with no free parameters, and the solid curve is a fit allowing an arbitrary normalization.

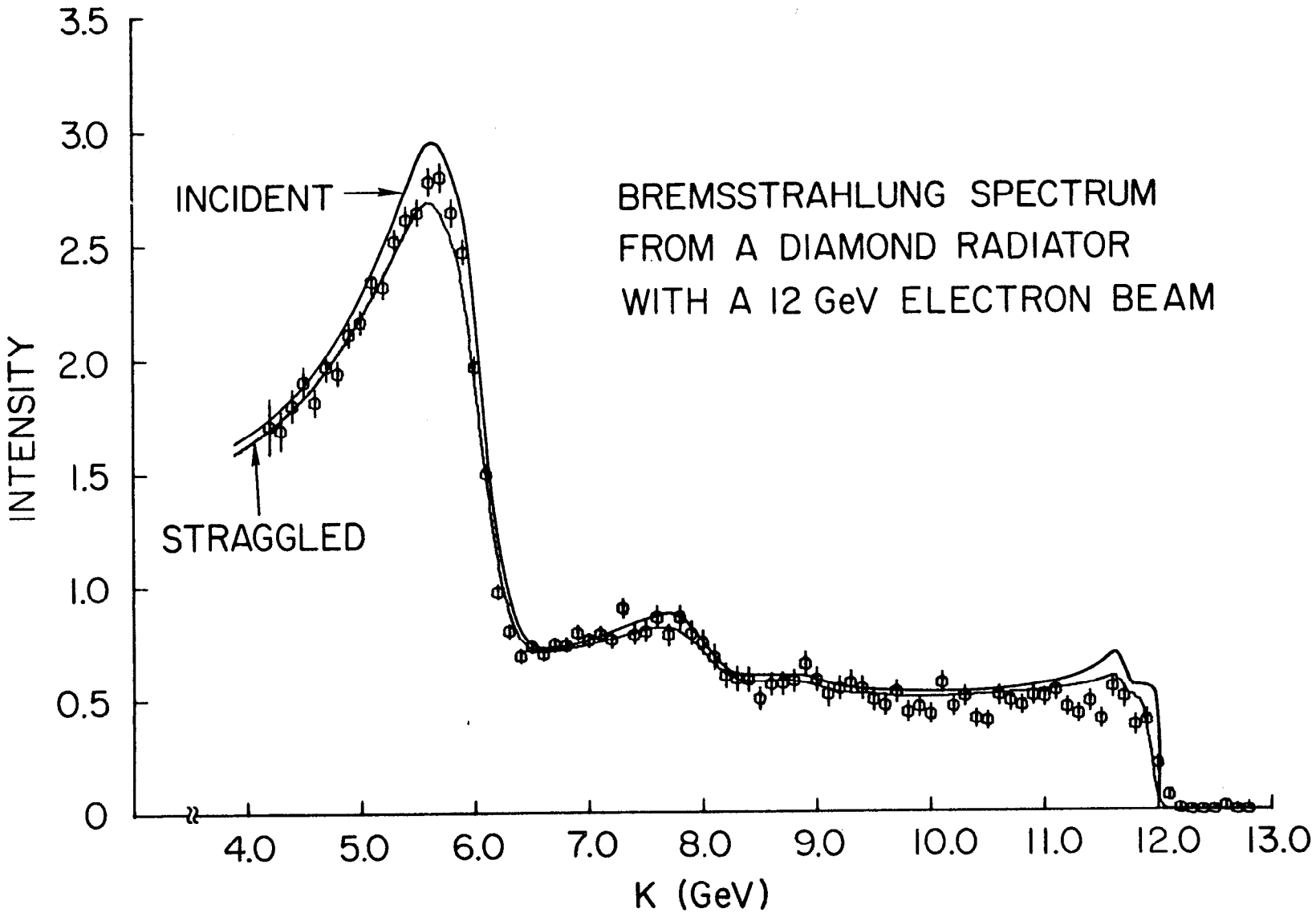
INCIDENT
STRAGGLED
BREMSSTRAHLUNG SPECTRUM
FROM A DIAMOND RADIATOR
WITH A 12 GeV ELECTRON BEAM
INTENSITY
K (GeV)
0
0.5
1.0
1.5
2.0
2.5
3.0
3.5
4.0
5.0
6.0
7.0
8.0
9.0
10.0
11.0
12.0
13.0

FIG. 1

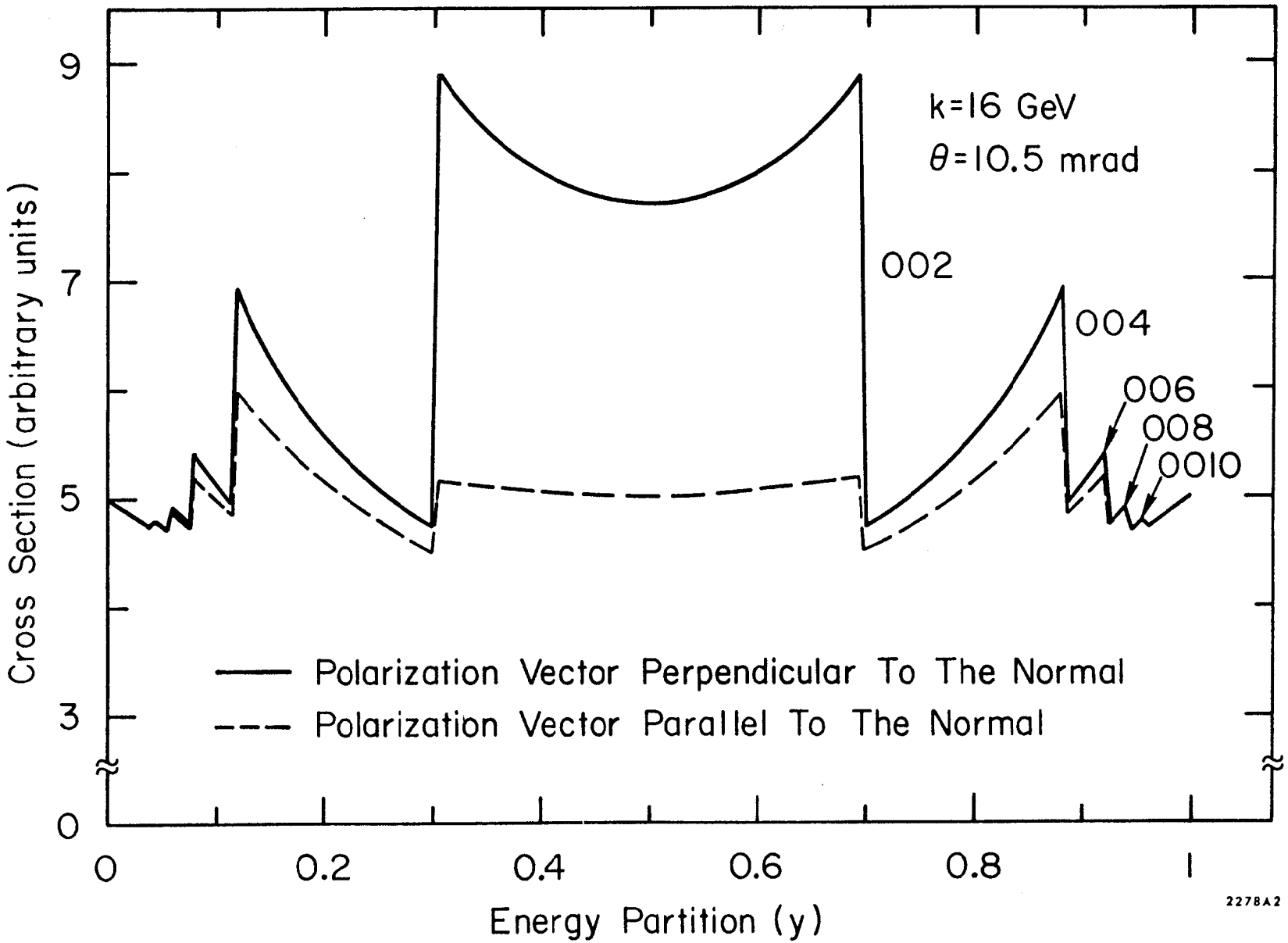
k=16 GeV
θ=10.5 mrad
002
004
006
008
0010
Polarization Vector Perpendicular To The Normal
Polarization Vector Parallel To The Normal
Cross Section (arbitrary units)
Energy Partition (y)
0
3
5
7
9
0
0.2
0.4
0.6
0.8
1
2278A2

FIG. 2

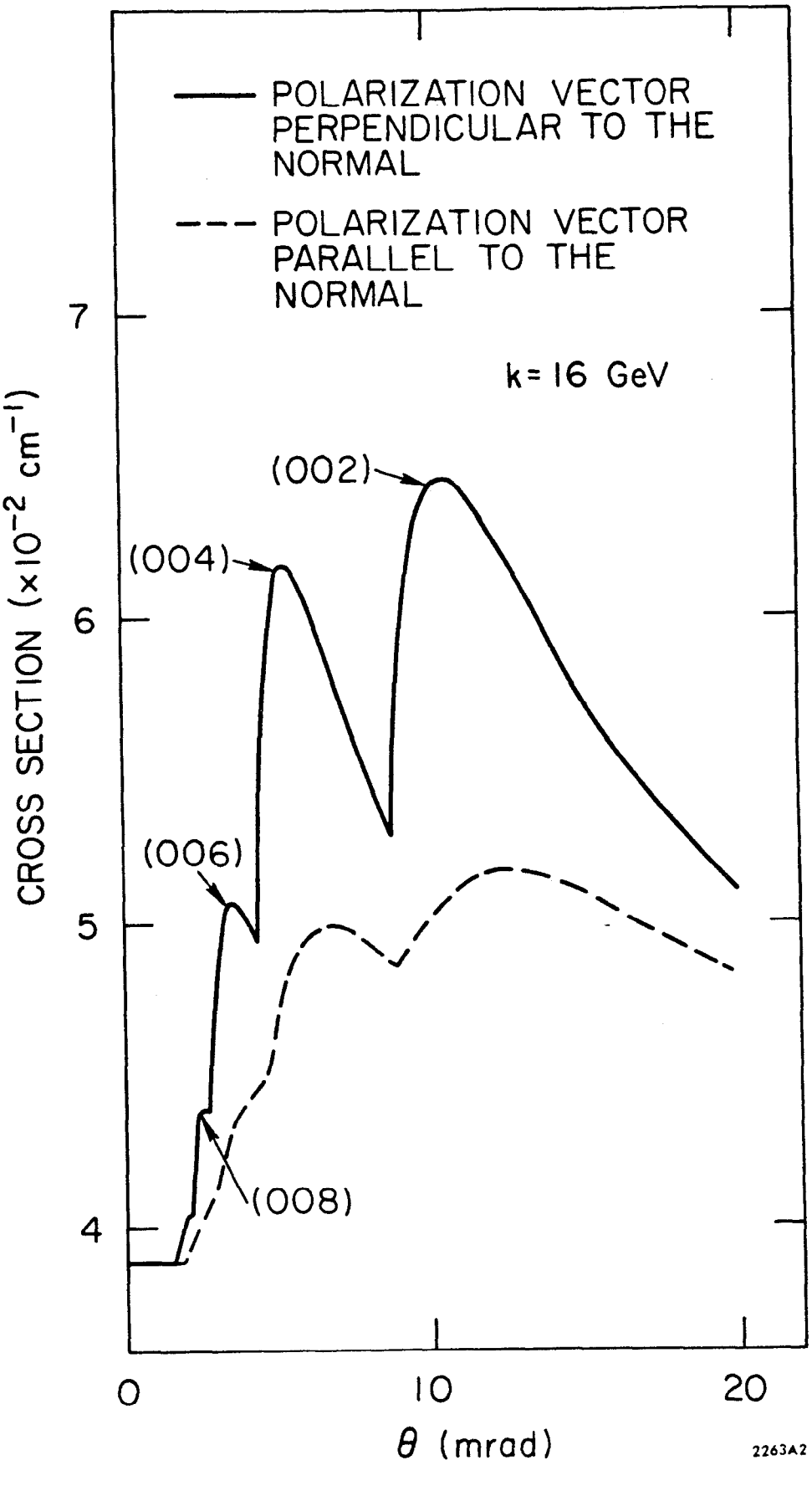
POLARIZATION VECTOR PERPENDICULAR TO THE NORMAL
POLARIZATION VECTOR PARALLEL TO THE NORMAL
k = 16 GeV
(002)
(004)
(006)
(008)
CROSS SECTION (×10⁻² cm⁻¹)
7
6
5
4
0
10
20
θ (mrad)
2263A2

FIG. 3

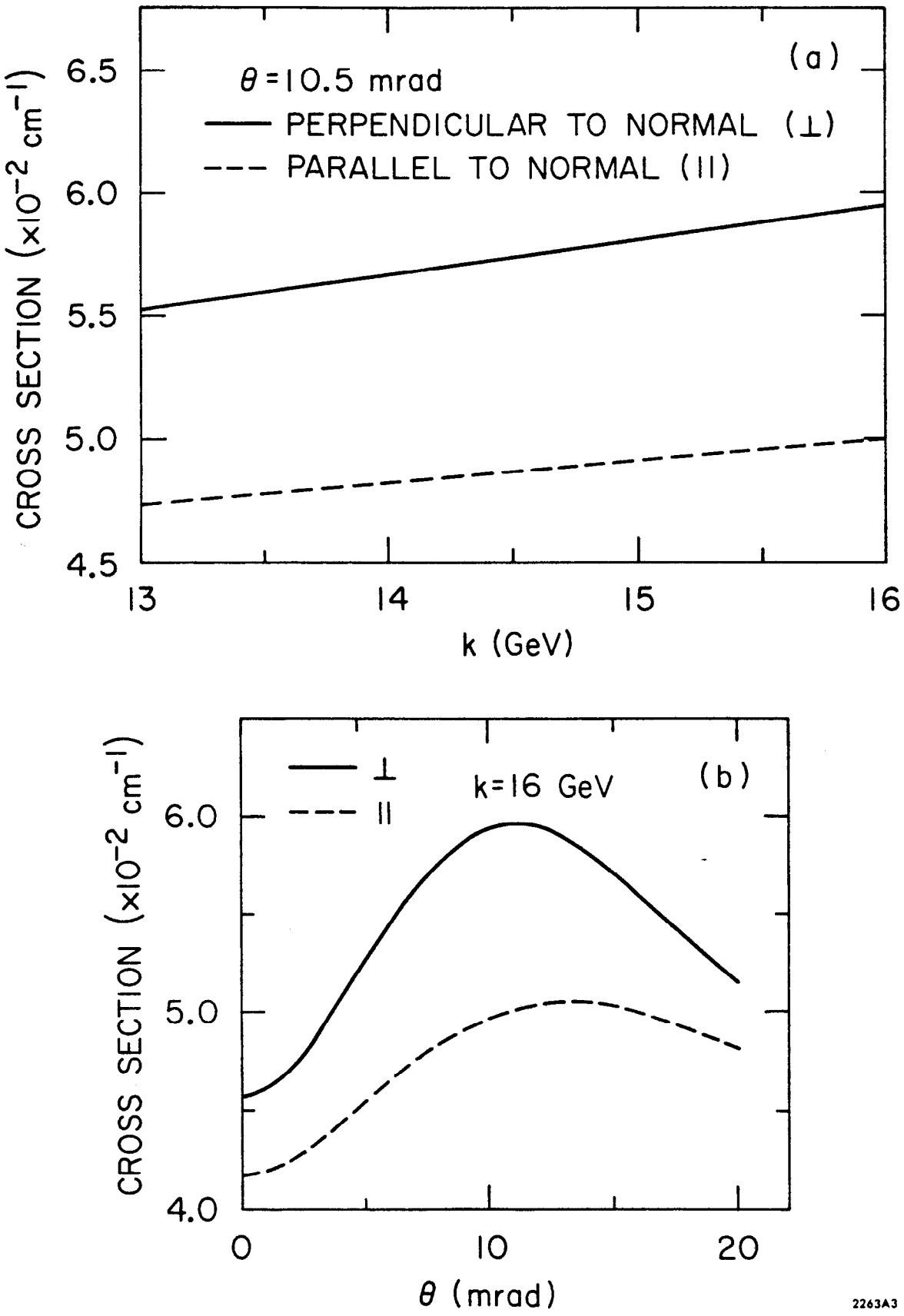
(a)
θ = 10.5 mrad
PERPENDICULAR TO NORMAL (⊥)
PARALLEL TO NORMAL (||)
CROSS SECTION (x10⁻² cm⁻¹)
6.5
6.0
5.5
5.0
4.5
13
14
15
16
k (GeV)
(b)
k = 16 GeV
⊥
||
CROSS SECTION (x10⁻² cm⁻¹)
6.0
5.0
4.0
0
10
20
θ (mrad)
2263A3

FIG. 4

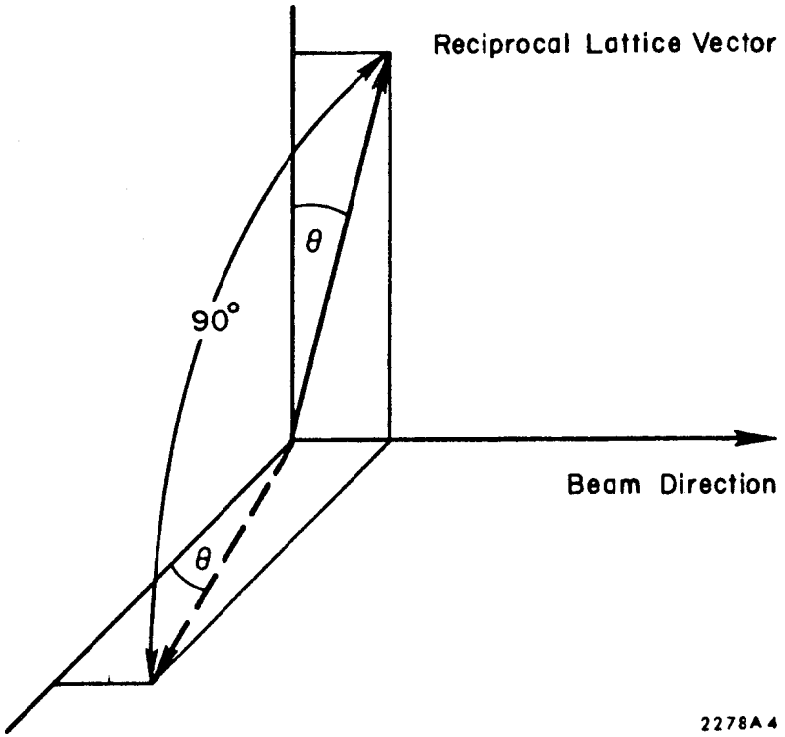

FIG. 5

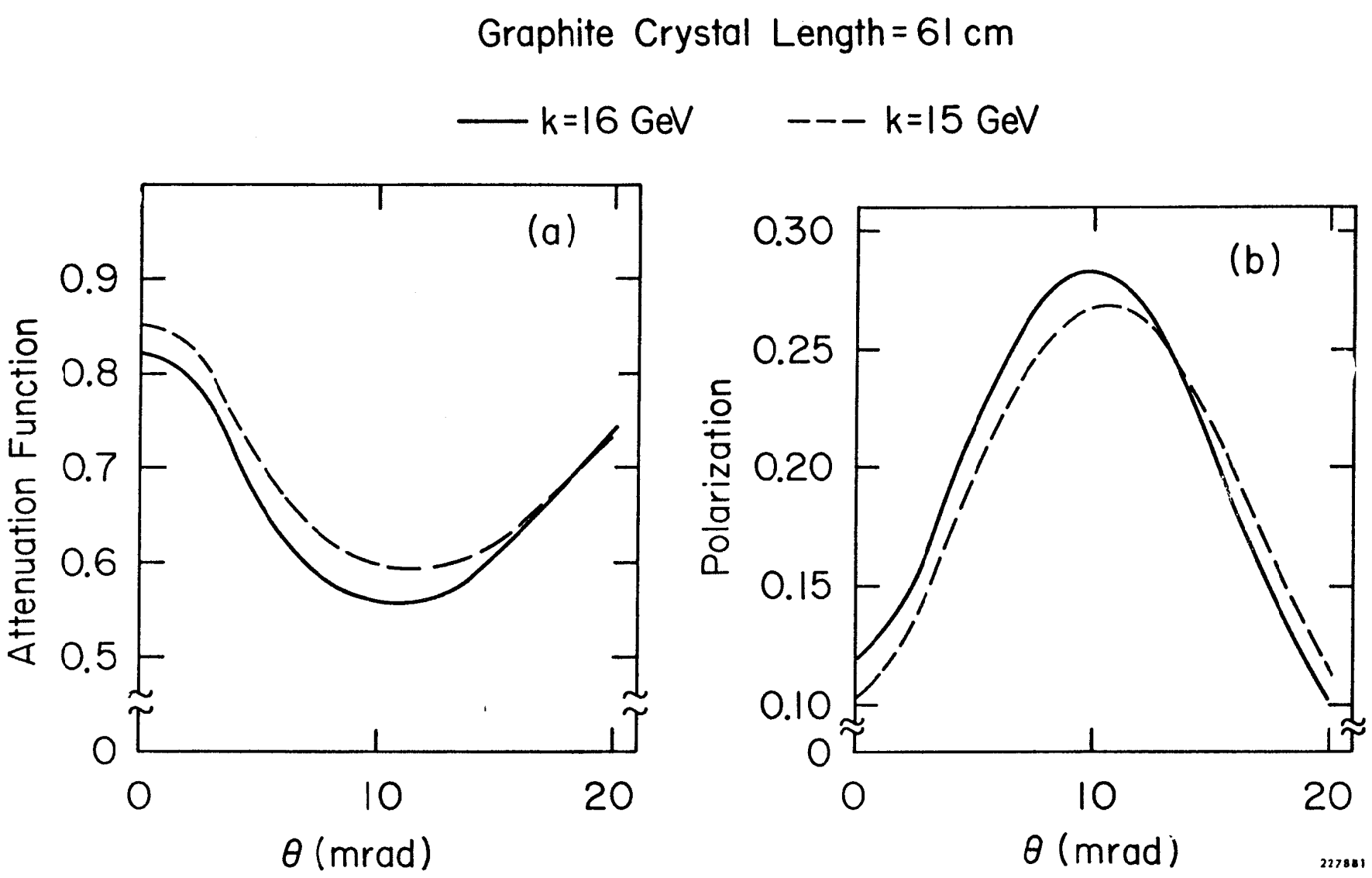
Graphite Crystal Length = 61 cm
k=16 GeV
k=15 GeV
(a)
Attenuation Function
0.9
0.8
0.7
0.6
0.5
0
0
10
20
θ (mrad)
(b)
Polarization
0.30
0.25
0.20
0.15
0.10
0
0
10
20
θ (mrad)
227881

FIG. 6

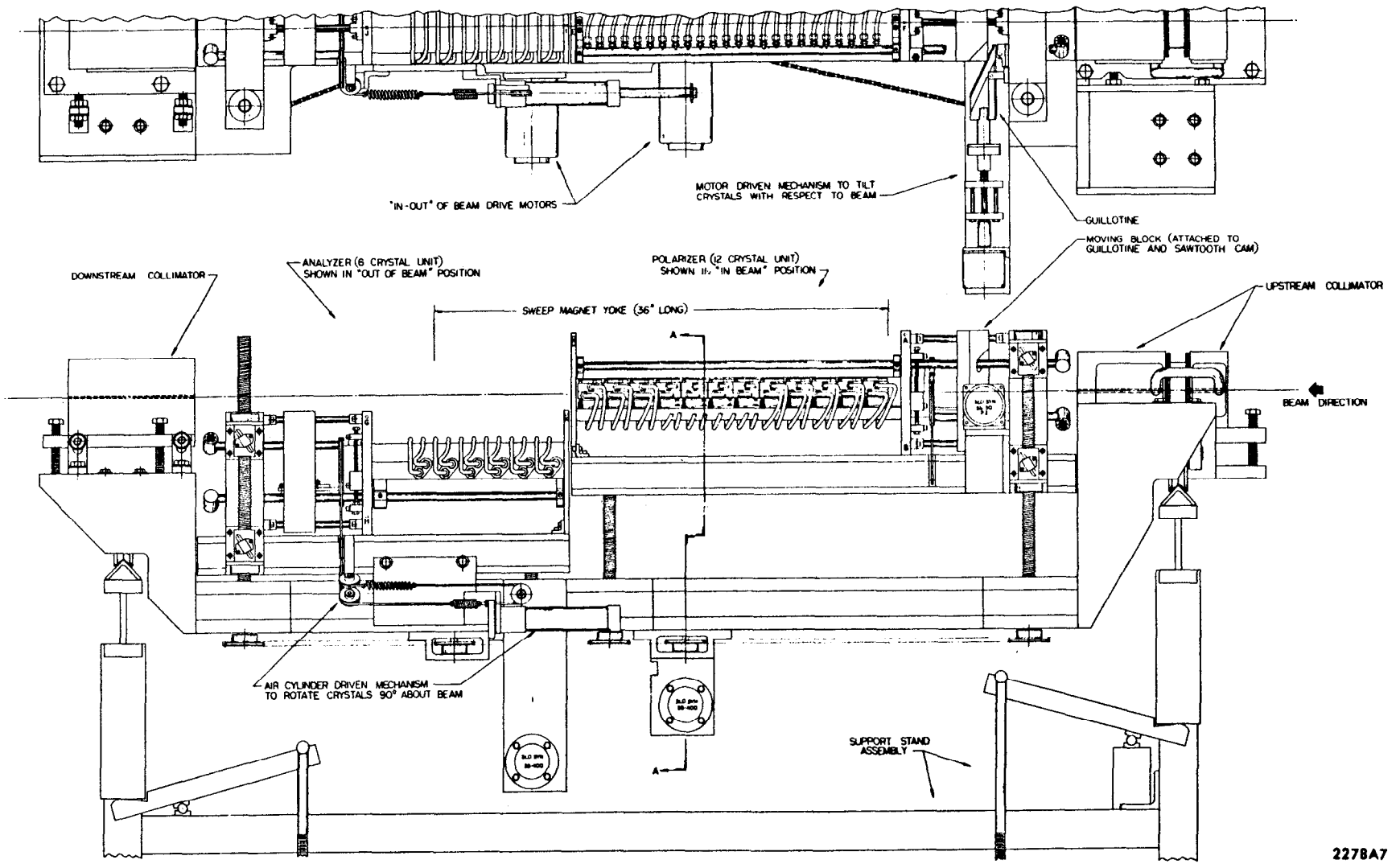
"IN-OUT" OF BEAM DRIVE MOTORS
MOTOR DRIVEN MECHANISM TO TILT CRYSTALS WITH RESPECT TO BEAM
GUILLOTINE
MOVING BLOCK (ATTACHED TO GUILLOTINE AND SAWTOOTH CAM)
DOWNSTREAM COLLIMATOR
ANALYZER (6 CRYSTAL UNIT) SHOWN IN "OUT OF BEAM" POSITION
POLARIZER (12 CRYSTAL UNIT) SHOWN IN "IN BEAM" POSITION
SWEEP MAGNET YOKE (36" LONG)
UPSTREAM COLLIMATOR
BEAM DIRECTION
AIR CYLINDER DRIVEN MECHANISM TO ROTATE CRYSTALS 90° ABOUT BEAM
SUPPORT STAND ASSEMBLY
2278A7

FIG. 7

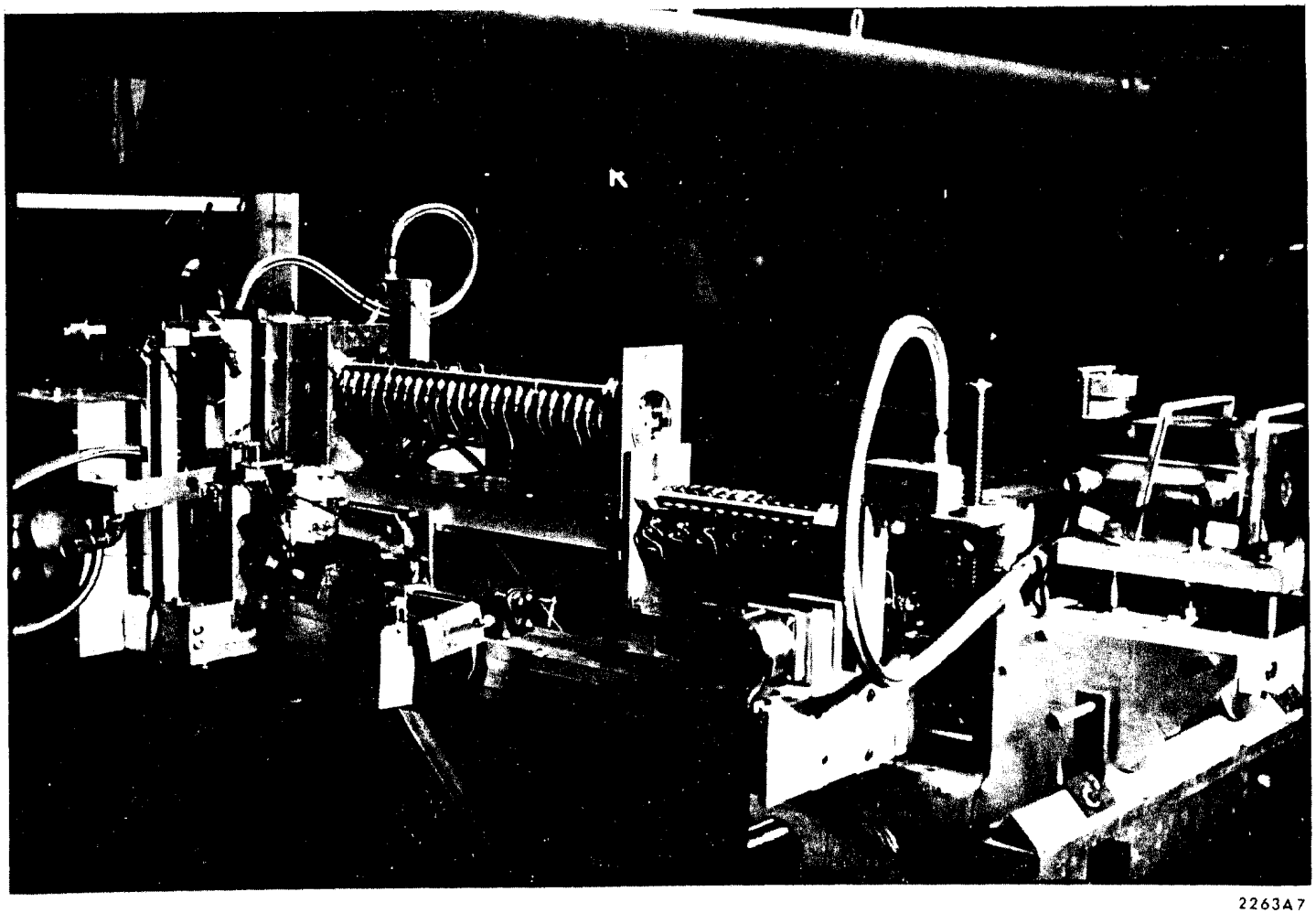

2263A7

FIG. 8

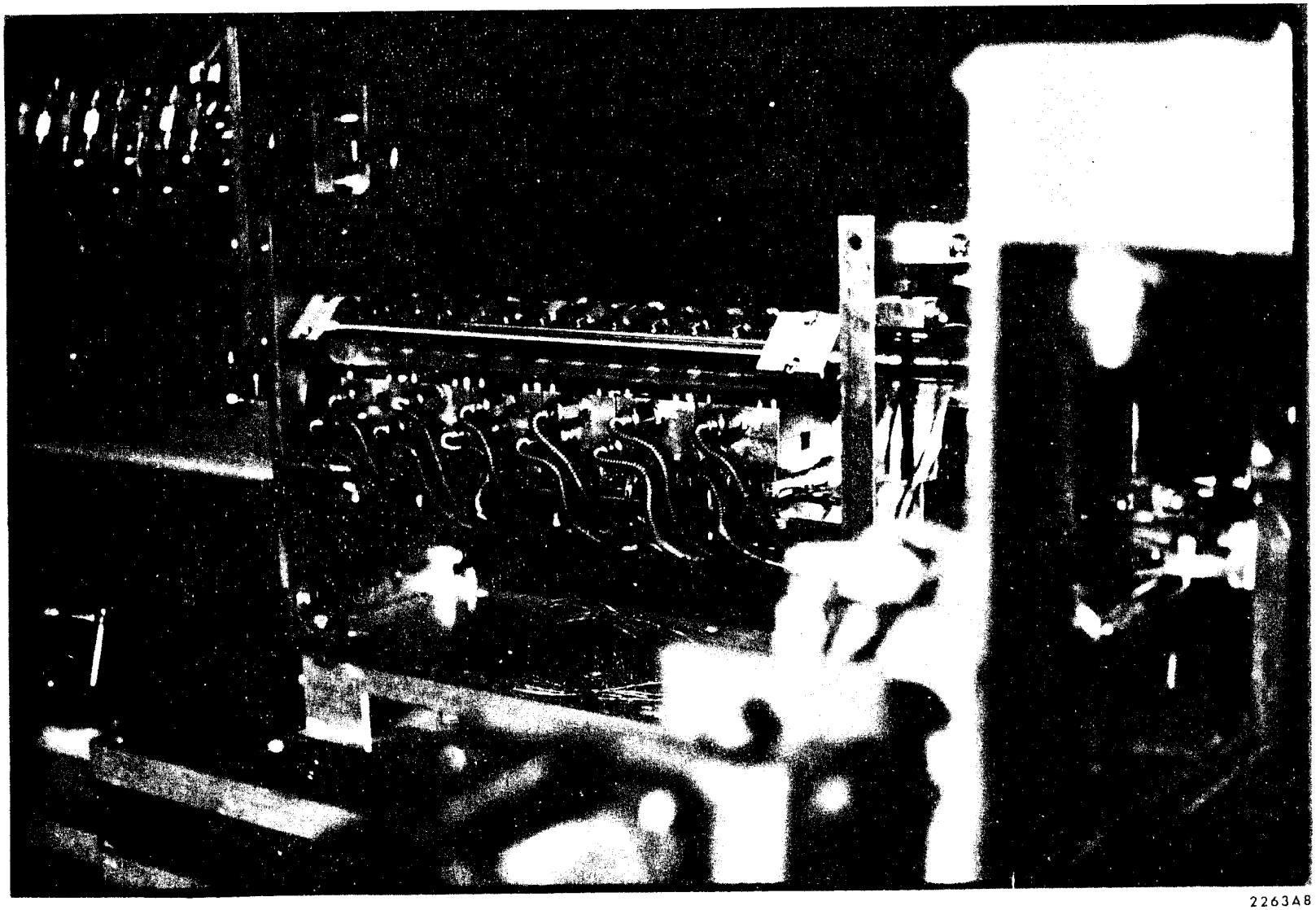

2263A8

FIG. 9

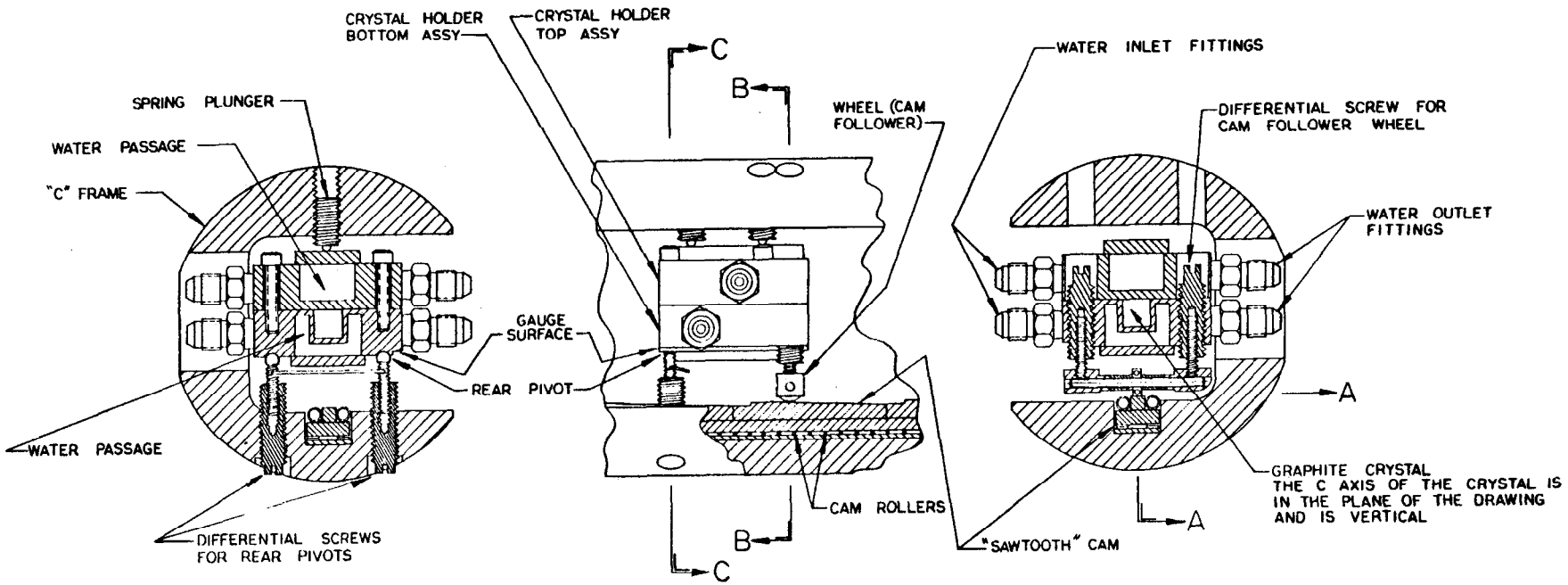
CRYSTAL HOLDER BOTTOM ASSY
CRYSTAL HOLDER TOP ASSY
C
B
WHEEL (CAM FOLLOWER)
WATER INLET FITTINGS
DIFFERENTIAL SCREW FOR CAM FOLLOWER WHEEL
SPRING PLUNGER
WATER PASSAGE
"C" FRAME
WATER OUTLET FITTINGS
GAUGE SURFACE
REAR PIVOT
A
WATER PASSAGE
GRAPHITE CRYSTAL THE C AXIS OF THE CRYSTAL IS IN THE PLANE OF THE DRAWING AND IS VERTICAL
CAM ROLLERS
B
A
"SAWTOOTH" CAM
DIFFERENTIAL SCREWS FOR REAR PIVOTS
C
SECTION C-C
SECTION A-A
SECTION B-B
2263A9

FIG. 10

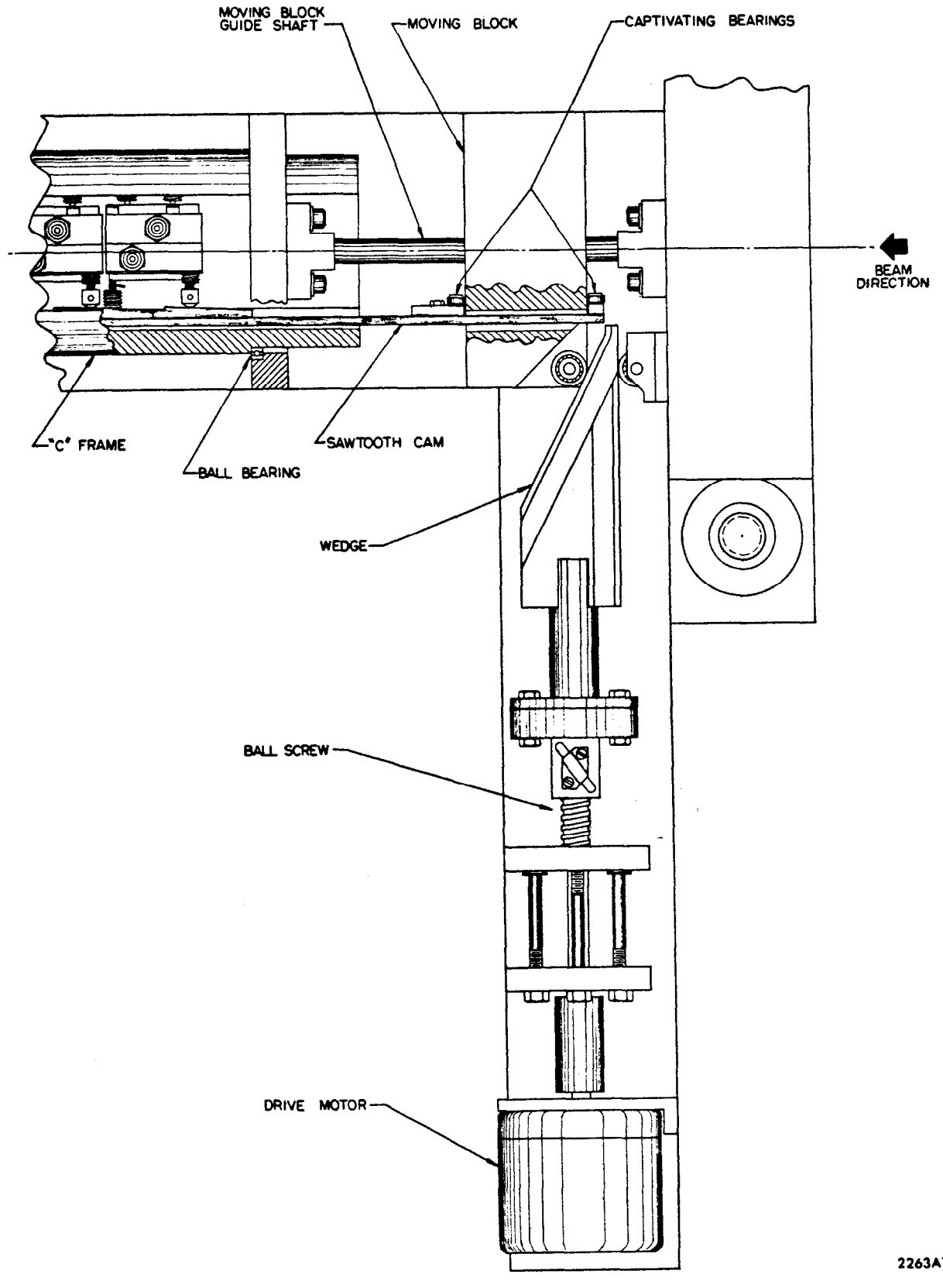
MOVING BLOCK GUIDE SHAFT
MOVING BLOCK
CAPTIVATING BEARINGS
BEAM DIRECTION
"C" FRAME
BALL BEARING
SAWTOOTH CAM
WEDGE
BALL SCREW
DRIVE MOTOR
2263A10

FIG. 11

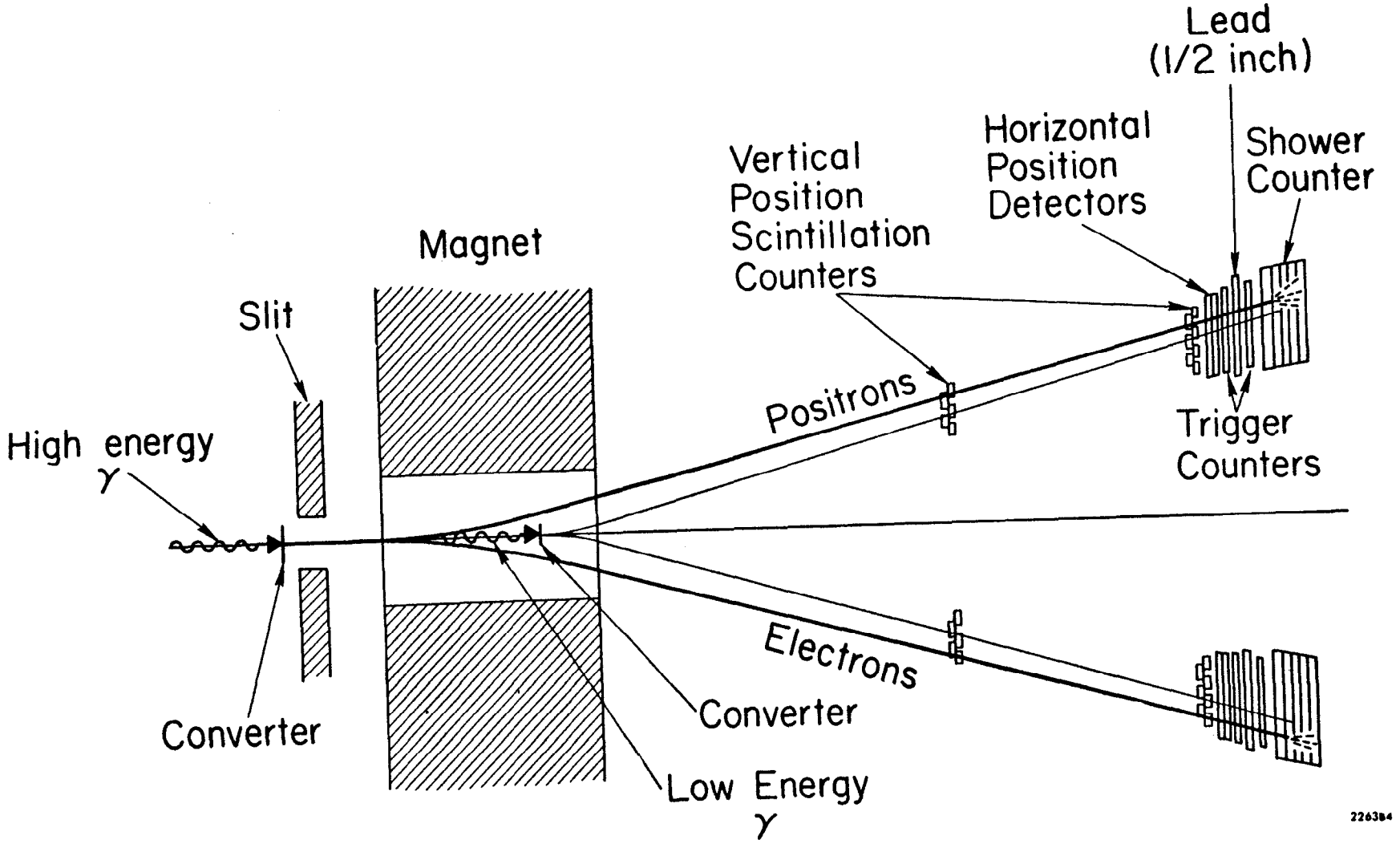
Lead
(1/2 inch)
Horizontal
Position
Detectors
Shower
Counter
Vertical
Position
Scintillation
Counters
Magnet
Slit
Positrons
High energy
γ
Trigger
Counters
Electrons
Converter
Converter
Low Energy
γ
226384

FIG. 12

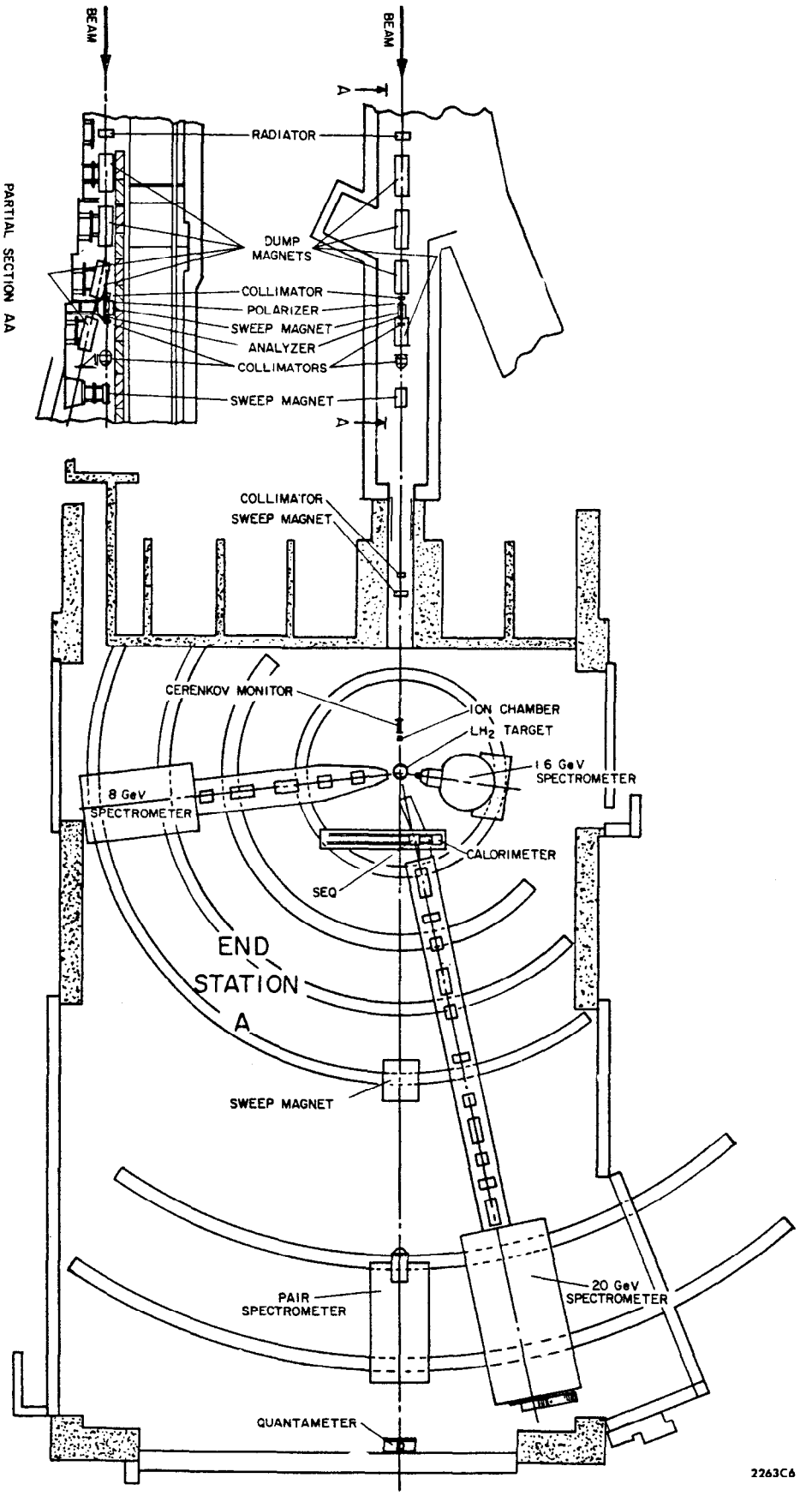
BEAM
BEAM
A
A
RADIATOR
DUMP MAGNETS
COLLIMATOR
POLARIZER
SWEEP MAGNET
ANALYZER
COLLIMATORS
SWEEP MAGNET
PARTIAL SECTION AA
COLLIMATOR
SWEEP MAGNET
CERENKOV MONITOR
ION CHAMBER
LH2 TARGET
16 GeV SPECTROMETER
8 GeV SPECTROMETER
CALORIMETER
SEQ
END STATION A
SWEEP MAGNET
PAIR SPECTROMETER
20 GeV SPECTROMETER
QUANTAMETER
2263C6

FIG. 13

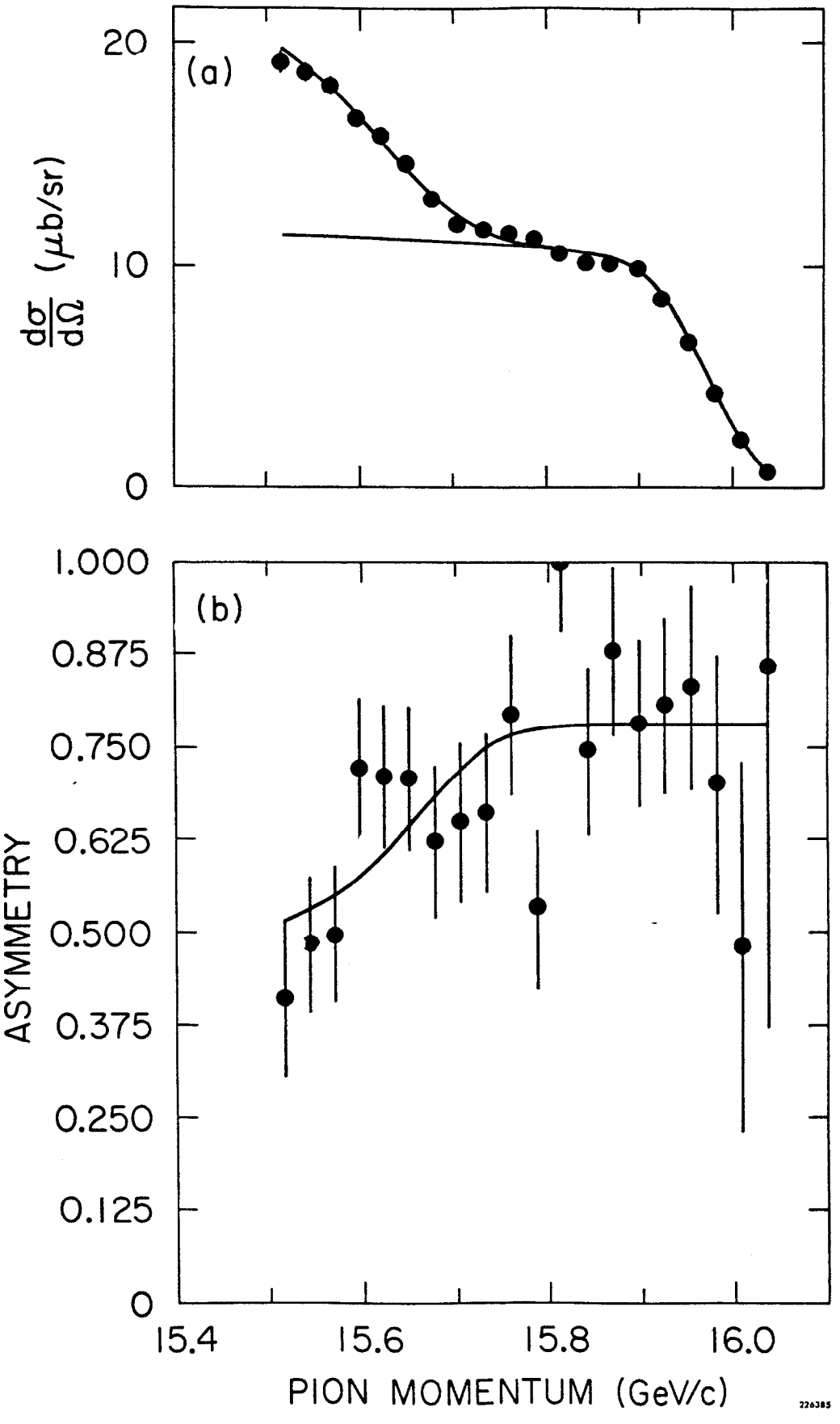
(a)
20
10
0
$\frac{d\sigma}{d\Omega}$ (μb/sr)
(b)
1.000
0.875
0.750
0.625
0.500
0.375
0.250
0.125
0
ASYMMETRY
15.4
15.6
15.8
16.0
PION MOMENTUM (GeV/c)
226385

FIG. 14

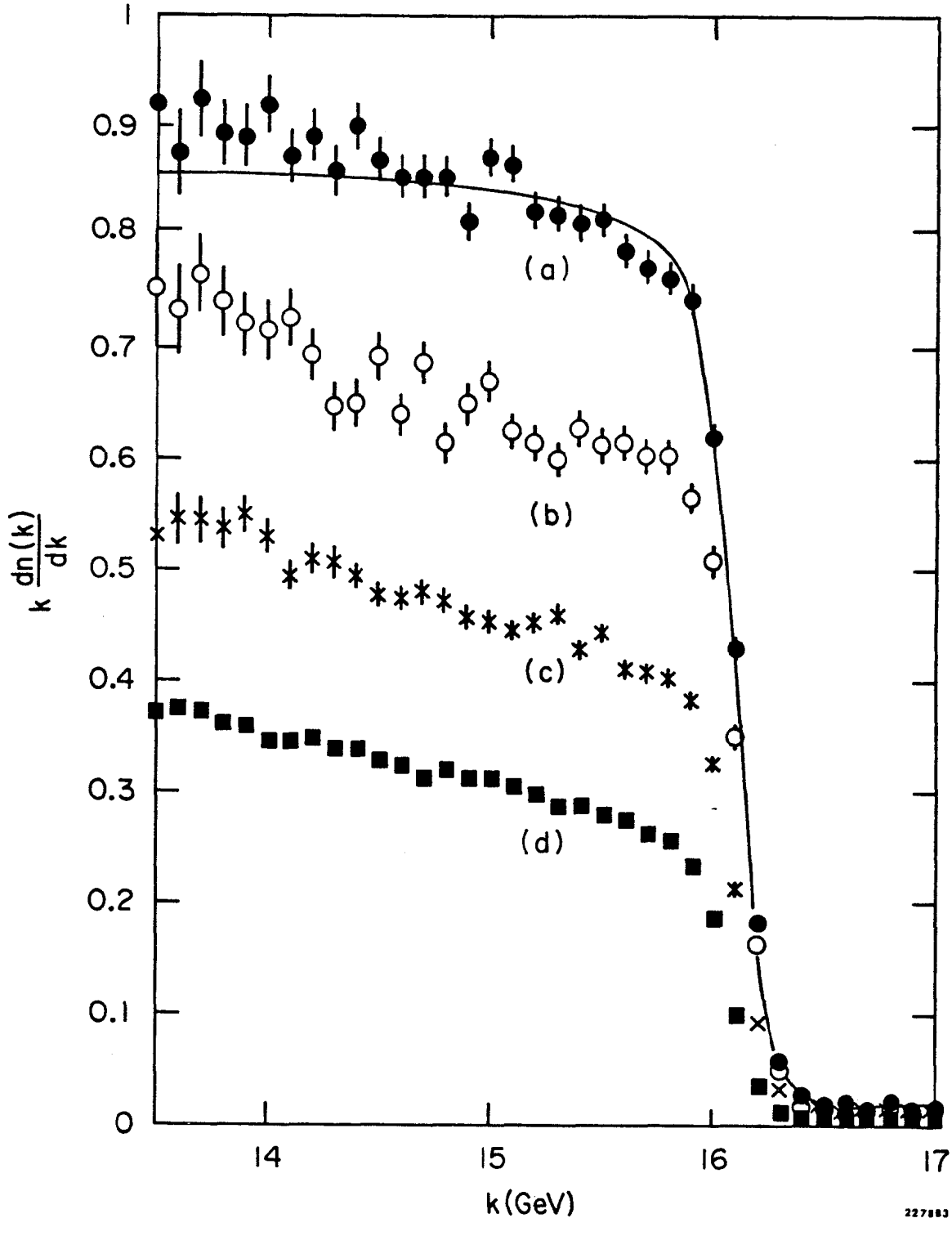
1
0.9
0.8
0.7
0.6
0.5
0.4
0.3
0.2
0.1
0
14
15
16
17
k(GeV)
$k\frac{dn(k)}{dk}$
(a)
(b)
(c)
(d)
227883

FIG. 15

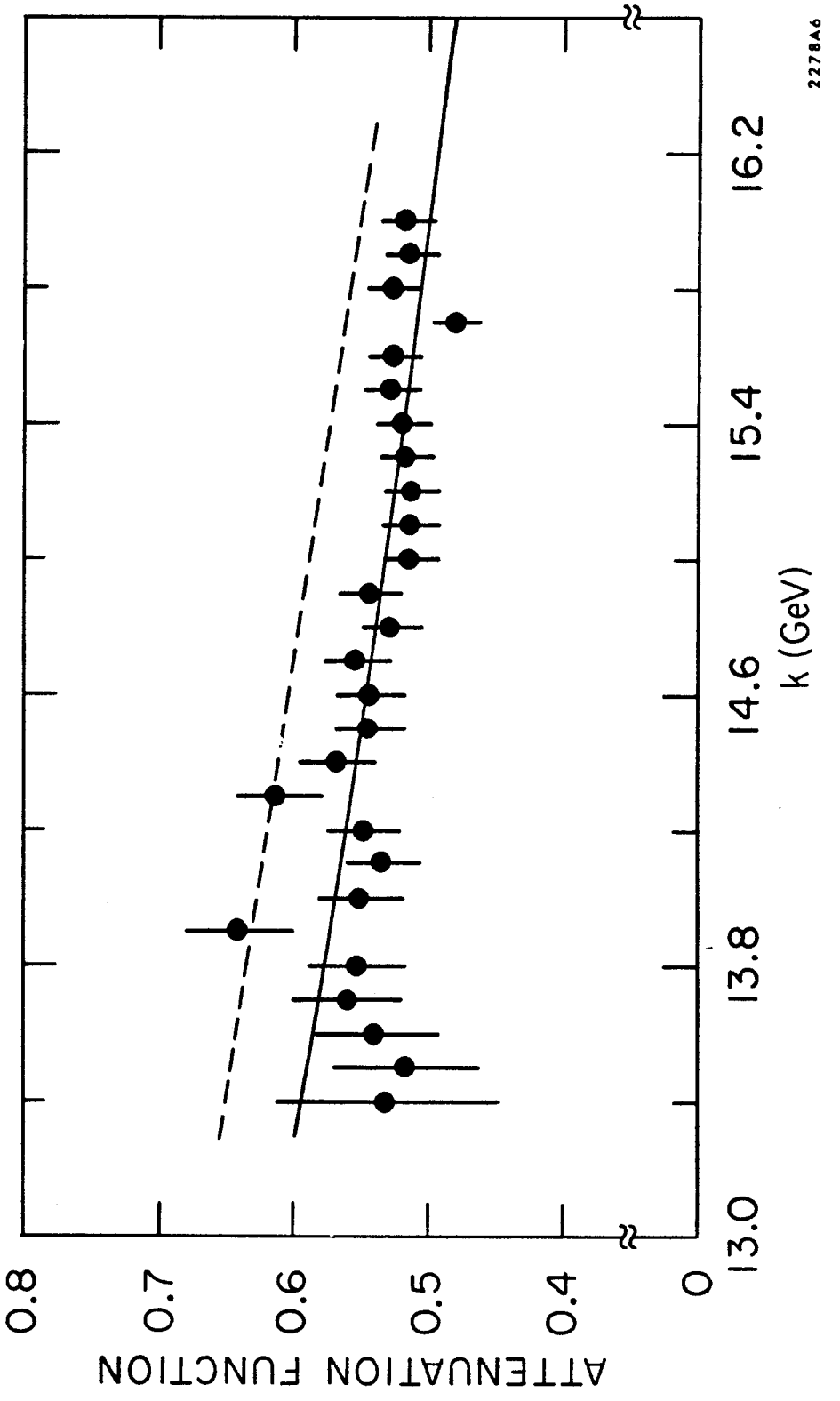
ATTENUATION FUNCTION
0.8
0.7
0.6
0.5
0.4
0
13.0
13.8
14.6
15.4
16.2
k (GeV)
2278A6

FIG. 16

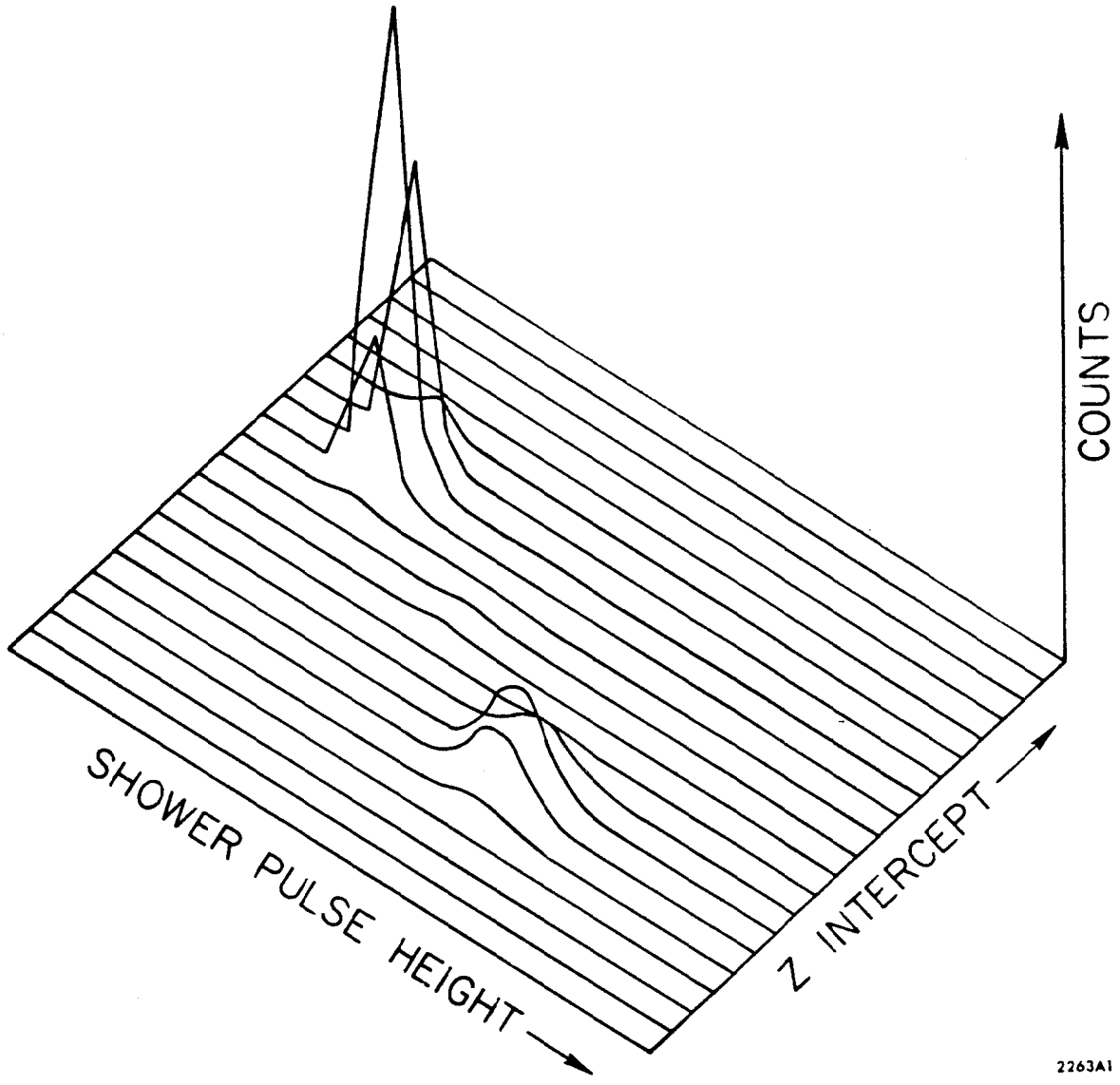

FIG. 17

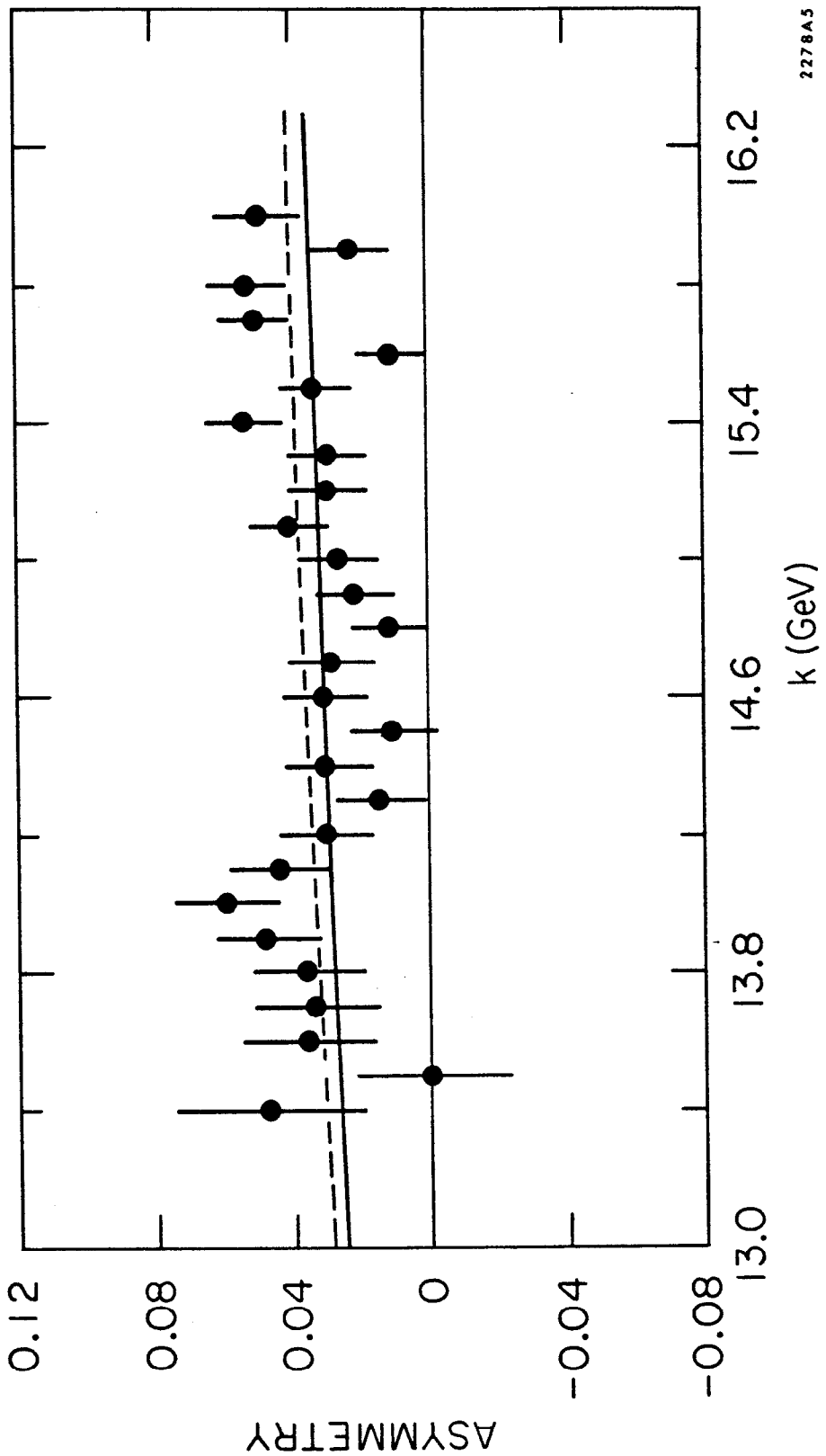
ASYMMETRY
0.12
0.08
0.04
0
-0.04
-0.08
13.0
13.8
14.6
15.4
16.2
k (GeV)
2278A5

FIG. 18